Pacific Northwest
NATIONAL LABORATORY

PNNL-30603

Modeling of fission and activation products in molten salt reactors and their potential impact on the radionuclide monitoring stations of the International Monitoring System

August 2020

Christine Johnson
Johnathan L. Slack
Manish K. Sharma
Cheslan K. Simpson
Jonathan L. Burnett

U.S. DEPARTMENT OF ENERGY

Prepared for the U.S. Department of Energy
under Contract DE-AC05-76RL01830

DISCLAIMER

PACIFIC NORTHWEST NATIONAL LABORATORY
operated by
BATTELLE
for the
UNITED STATES DEPARTMENT OF ENERGY
under Contract DE-AC05-76RL01830

Printed in the United States of America

Available to DOE and DOE contractors from the Office of Scientific and Technical Information,
P.O. Box 62, Oak Ridge, TN 37831-0062
www.osti.gov
ph: (865) 576-8401
fax: (865) 576-5728
email: reports@osti.gov

Available to the public from the National Technical Information Service
5301 Shawnee Rd., Alexandria, VA 22312
ph: (800) 553-NTIS (6847)
or (703) 605-6000
email: info@ntis.gov
Online ordering: http://www.ntis.gov

Modeling of fission and activation products in molten salt reactors and their potential impact on the radionuclide monitoring stations of the International Monitoring System

August 2020

Christine Johnson
Johnathan L. Slack
Manish K. Sharma
Cheslan K. Simpson
Jonathan L. Burnett

Prepared for
the U.S. Department of Energy
under Contract DE-AC05-76RL01830

Pacific Northwest National Laboratory
Richland, Washington 99354

Abstract

Molten Salt Reactors (MSRs) are one of six Generation IV reactor designs currently under development around the world. Because of the unique operating conditions of MSRs, which include molten fuel and the continuous removal of gaseous fission products during operation, work was performed to analyze the potential impact of emissions on the International Monitoring System (IMS) of the Comprehensive Nuclear-Test-Ban Treaty (CTBT). Simulations were performed to predict the production of IMS-relevant radionuclides in four MSR designs operating under two scenarios – (1) a sealed reactor with releases only during operational shutdown and (2) continuous reprocessing or sparging of the fuel salt. From these production estimates the radioxenon and radioiodine signatures were extracted and compared to three current reactor designs (PWR, BWR, RBMK). In the cases where continuous reprocessing of the fuel salt occurred both the radioxenon and radioiodine signatures are nearly indistinguishable from a nuclear explosion. Estimates were also made of the potential emission rate of radioxenon for three reactor designs and it was found that MSRs have the potential to emit radioxenon isotopes at a rate of 10^{15} – 8×10^{16} Bq/d for ^{133}Xe if no abatement is used. An assessment was also made of activation products using a candidate fuel salt (FLiBe) mixed with corrosion products for the Thorium Molten Salt Reactor (TMSR-LF1).

Acknowledgments

This research was funded by the National Nuclear Security Administration, Office of International Nuclear Safeguards (NNSA NA-241). The views expressed here do not necessarily reflect the opinion of the United States Government, the United States Department of Energy, or the Pacific Northwest National Laboratory. Pacific Northwest National Laboratory is operated for the U.S. Department of Energy by Battelle under Contract DE-AC05-76RL01830.

Acronyms and Abbreviations

ARE	Aircraft Reactor Experiment
BWR	Boiling Water Reactor
CMSR	Compact Molten Salt Reactor
CTBT	Comprehensive Nuclear-Test-Ban Treaty
DFR	Dual Fluid Reactor
FLiBe	Fluoride, Lithium, and Beryllium salt
FLiNaK	Fluoride, Lithium, Sodium, and Potassium salt
GIF	Generation IV International Forum
IFK	German Institute for Solid State Nuclear Physics
IMS	International Monitoring System
IMSBR	Indian Molten Salt Breeder Reactor
LFTR	Liquid Fluoride Thorium Reactor
LWR	Light-Water Reactor
MCFR	Molten Chloride Fast Reactor
MIPF	Medical Isotope Production Facility
MOSART	Molten Salt Actinide Recycler and Transmuter
MSBR	Molten Salt Breeder Reactor
MSR	Molten Salt Reactor
MSFR	Molten Salt Fast Reactor
MSRE	Molten Salt Reactor Experiment
MOX	Mixed Oxide
NPP	Nuclear Power Plant
ORIGEN	Oak Ridge Isotope Generation
PWR	Pressurized-Water Reactor
RBMK	Reaktor Bolshoy Moshchnosti Kanalnyy (High-Power Channel-Type Reactor)
RR	Research Reactor
TMSR	Thorium Molten Salt Reactor
TMSR-LF1	Thorium Molten Salt Reactor-Liquid Fuel 1
TRISO	TRistructural-ISOtropic
TRU	TRansUranics

Contents

Figures

Tables

1.0 Introduction

Molten salt reactors (MSRs) are one of six types of Generation IV nuclear reactor designs under consideration by the Generation IV International Forum (GIF) (Holcomb, 2017). There are a wide range of MSR designs with variations in their power output, footprint, fuel forms, salt types, coolant systems, fuel cycles, and capacity for breeding. MSRs come in two basic designs; those with solid fuel that use molten salt as a coolant and those in which the fuel is dissolved directly into the reactor salt. Solid fuel designs can have traditional fuel pellets inside rods but more often they have Tristructural-isotropic (TRISO) fuel pellets (Petti et al. 2006) arranged in pebble beds. Solid fuel designs have the advantage of industrial operational experience and simpler chemistry considerations. Liquid fuel designs offer online refueling by injecting a small amount of fuel directly into the fuel salt through an access port. This can greatly increase fuel utilization, reactor uptimes, and levels out reactor power curves.

The Molten Salt Reactor Experiment (MSRE), conducted at Oak Ridge National Laboratory, was the follow up experiment to the world's first molten salt reactor, the Airforce Reactor Experiment (ARE), also performed at ORNL (Haubenreich and Engel, 1970). The MSRE was a graphite moderated single-fluid design where the fissionable material (in this case 33% enriched ^{235}U as UF_6) was dissolved directly into the lithium, beryllium, zirconium, and uranium(IV) salt (65% ^{7}LiF, 29.1% BeF_4, 5% ZrF_4, 0.9% UF_4). Construction began in 1962 with the reactor going critical on ^{235}U by June 1st, 1965. Maximum power (thermal) output for the reactor was 7.4 MW which was then cooled using a similar base salt mixture (66% ^{7}LiF, 34% BeF_4, e.g. FLiBe) as the fuel salt via a heat exchanger. The MSRE had two operational campaigns, the first in June of 1965 where the reactor operated on ^{235}U, and the second from October 1968 to December of 1969 with ^{233}U (Rosenthal, 2010).

The success of the MSRE demonstrated the feasibility of molten salt reactors. A new concept, the Molten Salt Breeder Reactor (MSBR) began design and simulation studies at ORNL. The project was halted at the design phase and was officially ended in 1976. The discovery of rich deposits of natural uranium caused decreased interest in thorium reactor technology, of which the MSRE and MSBR was a part. (Rosenthal, 2010). However, the early successes at ORNL has inspired a comeback of the design in the US and internationally. There are currently five different reactor designs under development in the United States, most by private companies. There is also a bevy of research being conducted across multiple national laboratories investigating molten salt physical and chemical properties, salt cleanup techniques, reactor neutronics, etc. Research and development is progressing in China, Russia, the UK, India, Canada, Denmark, and a collaborative effort across multiple members of the European Union. China is currently the farthest along in the concept-to-criticality path with a liquid fuel test reactor, TMSR-LF1, scheduled for operation in 2020 (Chen et al., 2019). Table 1 summarizes some of the various reactor designs and where they are being developed.

Table 1. Summary of various countries experimental accomplishments and MSR concepts that are currently in development.

Country	Reactor Name/ Designation	Development Status	Target completion date	Fuel Type	Salt Type	Power
China	TMSR-SF0 Simulator molten salt reactor	Completed	2019, June	None	FLiNaK	N/A
China	TMSR-SF1 Thorium molten salt reactor – solid fuel	Under Construction	2020	Solid with TRISO particles	Primary FLiBe Secondary FLiNaK	10MW_{th}
China	TMSR-LF1 Experimental Reactor – liquid fuel	Under Construction	2020	Liquid Th/U	LiF-BeF_2-ZrF_4-UF_4-ThF_4	2MW_{th} (Chen et al., 2019)
China	TMSR-LF2 Multi-Purpose Research Reactor	Planning	2025	Liquid Th/^{233}U	TBA	20MW_e
China	TMSR-LF150 Small Modular Demonstration Reactor	Planning	2030	Liquid Th/U	TBA	150MW_{th}
Russia	MOSART Fuel Recycler /Transmuter	Design/ Simulation	2033 (10MW_{th} test reactor)	Liquid TRU/ LWR/ Th/^{233}U	15LiF-27BeF_2-58NaF	2400MW_{th}
USA (TerraPower)	MCFR Molten Chloride Fast Reactor	Design/ Testing	2023-2028	LEU/ Th/^{233}U	Chloride Based	30-150MW_{th}
USA (Kairos Power)	KP-FHR Kairos Power Fluoride salt High-Temp Reactor	Design/ Testing/ Pre-Licensing	2030	TRISO	FLiBe	140MW_e
USA (Flibe Energy)	LFTR Liquid-Fluoride Thorium Reactor	Design/ Development	TBA	Th/^{233}U	LiF-BeF2-UF4	600MW_{th}
USA (Elysium Industries)	MCSFR Molten Chloride Salt Fast Reactor	Design/ Development	2025	TRU/ LEU/ Th/^{233}U	Chloride Based	110 – 2700MW_{th}
USA	SmAHTR Small Advanced	Design/ Development	TBA	TRISO	FLiBe	125MW_{th}

	High-Temp Reactor					
Germany	DFR Dual Fluid Reactor	Design/ Simulation	2028	TRU/ LEU/ Th/^{233}U	Chloride Fuel Salt - Lead Coolant	3,000MW$_{th}$
Czech Republic	Energy Well Small Modular Molten Salt Cooled	Planning/ Technology Development	TBA	TRISO	TBA	20MW$_{th}$
Estonia	SMR Commercial small modular reactors	Feasibility/ Technology Selection	2030's	Solid fuel bundles	Moltex or Terra-Power based	Variable
Euratom	MSFR Molten Salt Fast Reactor	Laboratory Demo's/ Licensing	TBA	Liquid TRU/ Th/^{233}U	Fluorine based	3000MW$_{th}$
India	IMSBR Molten salt Breeder reactor	Planning/ Simulation	TBA	Th/^{233}U	TBA	850MW$_{e}$
India	IHTR Innovative High Temp Reactor	Planning/ Technology Development	TBA	TRISO	FLiNaK	600MW$_{th}$
Canada (Terrestrial Energy)	IMSR Integral Molten Salt Reactor	Design Review/ Site Selection	2028	Liquid LEU	Fluorine based	195 MW$_{e}$
Denmark (Seaborg Technologies)	CMSR Compact Molten Salt Reactor	Design Review/ Licensing	2027	Liquid TRU/ Th/^{233}U	Fluorine based	50MW$_{th}$
United Kingdom (Moltex)	SSR Stable Salt Reactor(s)	Design Review/ Licensing	2030	MOX/ Th/^{233}U TRU	Chloride or Fluoride	150MW$_{th}$
United Kingdom	AGR-FHR Fluoride-cooled high-temperature reactor	Preconceptual Design	TBA	TRISO	Primary FLiBe Secondary FLiNaK	TBA

The unique Generation IV design may have implications for global nuclear explosion monitoring efforts that measure trace-level radionuclides against a background of emissions from legitimate nuclear sources such as nuclear power plants (NPPs), research reactors (RRs) and medical isotope production facilities (MIPFs). Short-lived gaseous and volatile radionuclides may more readily escape from the molten fuels and coolants, producing emissions with a different isotopic signature to existing sources. This effect could be further enhanced by the online removal of accumulating fission products in MSR designs. In particular, this could interfere with the particulate and gaseous measurements performed by the International Monitoring System (IMS) that supports the Comprehensive Nuclear-Test-Ban Treaty (CTBT). The CTBT bans any nuclear weapon test explosion or any other nuclear explosion (UN, 1996), and consists of 321 monitoring stations and 16 laboratories distributed around the world. Eighty of these stations are

focused on the collection and analysis of radioactive particulates, and 40 of these radionuclide stations include co-located radioxenon detection systems. The IMS aims to provide a 90% probability of detecting a 1 kT nuclear explosion within 14 days (Medici, 2001; Schulze et al., 2000). Particulate monitoring stations perform gamma-spectroscopy measurements on air-filters for 84 activation and fission products (Bowyer et al., 1997; Burnett, 2019; Miley et al., 1998). Noble gas stations perform measurements, either through beta-gamma coincidence or gamma-spectroscopy, on processed air samples for 4 radioactive isotopes of xenon (^{131m}Xe, ^{133}Xe, ^{133m}Xe, ^{135}Xe) (Bowyer et al., 2002; Fontaine et al., 2004; Kalinowski et al., 2010; Ringbom et al., 2003). A thorough assessment of the potential impact of MSR emissions on these isotopes of interest should be completed before these systems begin operating around the globe.

Herein, we present our findings on how the multitude of MSRs currently under development will affect the landscape of monitoring for the CTBTO isotopes of interest. Simulations are run on four different categories of MSR's to build isotope activities/ratios for xenon (^{131m}Xe, ^{133}Xe, ^{133m}Xe, ^{135}Xe) and iodine (^{131}I, ^{133}I, ^{135}I) isotopes that are then compared to civilian sources such as NPPs and RRs. Tables of the 17 key CTBTO isotopes are produced with activities from reactors that are representative of the different MSR base designs. Activity values (in Bq) for all 84 CTBT isotopes of interest, including fission and activation products, taken at 180 and 300 days of continuous operation are given in **Error! Reference source not found.**.

1.1 MSR Design Details

MSR concepts are highly varied based on design intent but for this work can be generally narrowed down to four categories (Table 2) based on neutron spectrum (thermal, intermediate, fast), the utilization of transuranic (TRU) or mixed-oxides(MOX) as fuel, and presence of a blanket fluid. For this work, one reactor design was chosen from each category and is shown in bold in Table 2: the Thorium Molten Salt Reactor (TMSR-LF1), the Molten Salt Breeder Reactor (MSBR), the Molten Salt Actinide Recycler & Transmuter (MOSART) reactor, and the Dual Fluid Reactor (DFR). Simplified schematic representations of each type are presented in the figures below.

Table 2. Description of the four general MSR types examined in this work. Reactor names in bold are those simulated in this work.

Reactor Category	Neutron Spectra	Thorium Breeding	TRU or MOX Burning	Examples	References
Graphite Moderated Thermal	Thermal	Optional (thorium in the fuel salt)	Potential	MSRE (USA) **TMSR (China)** ThorConIsle (USA)	(Haubenreich and Engel, 1970) (Zhou et al., 2020b) (Lumbanraja and Liun, 2018)
Graphite Reflected Fast	Intermediate/Fast	Optional	Yes	**MOSART (Russia)** MSFR (EU) MCFR (USA)	(Ignatiev et al., 2015) (Sgro, 2018)
Dual Fluid Thermal	Thermal	Optional (thorium in a blanket salt)	Potential	LFTR (USA) CMSR (Denmark) **MSBR (USA)**	(IAEA, 2016) (Pater, 2019) (Rosenthal et al., 1972)
Dual Fluid Fast	Intermediate/Fast	Optional	Yes	IMSBR(India) **DFR (Germany)**	(VIJAYAN et al., 2015) (Huke et al., 2015)

The graphite moderated thermal reactors are closest to the original ORNL MSRE design. They feature a reactor core that contains a graphite moderator with salt channels, as shown in Figure 1. Fuel salt (orange) flows through the channels in the graphite (yellow) producing a thermal neutron spectrum. These reactors are primarily used for generating power and process heat, but breeding can be accomplished by injecting the thorium stock into the fuel salt. The resulting ^{233}Pa would then need to be separated from the fuel salt via pyroprocessing techniques and

kept out of circulation until it decays into ^{233}U. The TMSR-LF1 is an example of this reactor class and is scheduled for operation in 2020 (Chen et al., 2019).

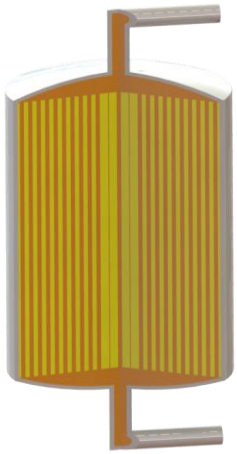

Figure 1. Simplified schematic of a graphite moderated thermal reactor such as the MSRE and TMSR. Orange areas represent fuel salt and yellow areas represent graphite.

Graphite reflected fast reactors have a hollow reactor core (orange) that is lined on the outer perimeter with a graphite reflector (yellow). This configuration, shown in Figure 2, results in a fast neutron spectrum. The primary intent of these reactors is to transmute or burn transuranic (TRU) or mixed oxide (MOX) fuels while having the option to breed ^{232}Th, or ^{238}U. The MOSART reactor was designed from the ground up for this purpose and is an excellent example of this type of MSR design (Pater, 2019).

Figure 2. Simplified schematic of a graphite reflected fast burner reactor such as MOSART. Orange areas represent fuel salt and yellow areas represent graphite.

Dual fluid thermal designs have a primary fuel salt and a breeding salt known as the “blanket” salt (green) that surrounds either a hollow reactor core (yellow) or a salt channel core (orange) as shown in Figure 3. These reactors are graphite moderated with fuel salt channels and are well suited to breeding thorium due to their thermal spectrum. Having the blanket salt separated from the primary fuel salt simplifies the chemical processing needed to extract the ^{233}Pa. FLiBe

Energy's LFTR reactor design is the most notable example of this reactor type. The intent of the LFTR is to move quickly from startup operations with ^{235}U to sustained operations with ^{233}U that is bred in the blanket salt from thorium.

While it does technically fit in the dual fluid thermal category by virtue of the fact that it has two fluids and a thermal neutron spectrum, the CMSR by Seaborg Technologies is notable in that it does not have a blanket salt or use graphite moderation. Instead the CMSR uses molten NaOH as a fluid moderator between fuel salt channels in order to achieve a thermal neutron spectrum.

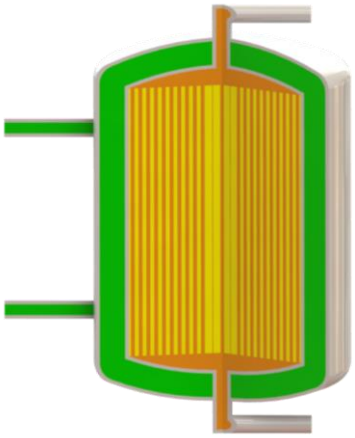

Figure 3. Simplified schematic of a dual fuel graphite moderated thermal reactor such as the LFTR. Orange areas represent fuel salt, yellow areas represent graphite, and green represents blanket salt.

Dual fluid fast reactors are essentially a dual fluid thermal reactor without a graphite moderated core. These designs feature graphite reflectors (yellow) along the perimeter of the core as well as a blanket salt that flows along the outside (green) as shown in Figure 4. These reactors can be used to breed thorium in the blanket salt while utilizing plutonium or ^{238}U in the fuel salt because of their fast neutron spectrum. This also makes them well suited to transmuting or burning TRU/MOX (Heuer et al., 2014) The Indian Molten Salt Breeder Reactor (IMSBR) is a straightforward example of this type of design. The IMSBR development program is part of a larger effort in India to use the spent fuel from current nuclear reactors in next generation breeder reactors to produce ^{233}U from thorium (VIJAYAN et al., 2015).

Germany's Dual Fluid Reactor (DFR) has a slightly different arrangement than the IMSBR. The DFR uses liquid lead as a coolant and has channels running through the core as well as around the reactor core. This has the effect of the lead operating as the primary heat exchange and neutron moderator. This design gives the DFR a broad neutron spectrum so that it can be used for breeding, transmuting, or waste elimination. The German Institute for Solid State Nuclear Physics (IFK) team has come up with two main designs, one with molten salt as a fuel and the other with molten metal (Wang et al., 2019).

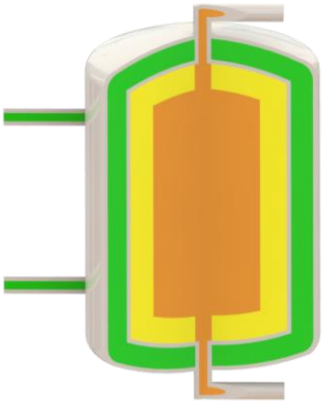

Figure 4. Simplified schematic of a dual fluid graphite reflected fast breeder reactor such as the DFR

1.1.1 Sparging

Some MSR designs include considerations for removing gaseous isotopes to reduce the effects on neutron poisons, such as ^{135}Xe. These poisons are not salt soluble and can be extracted from the fuel salt by introducing microscopic air pockets, typically by injecting helium, and then stripping the gas out of the fuel salt. This process is referred to as sparging and is meant to extract krypton, xenon, and tritium. Depending on the sparging system design, the off-gas will then be cleaned of these nuclides by charcoal filters or cryogenic trapping. In the MSRE a multitude of isotopes were found in gas samples (Zr, C, Cs, Nd, Nb, Mo, Ag, Ru, Te, I) taken in the off-gas system because of a fine mist generated by the pressurized jets that were used to force helium entrainment into the surface of the fuel salt (Compere et al., 1975). It was estimated that fuel salt was lost to the off-gas line in the form of mist at a rate of a few grams per month. The only other nuclides found in small quantities in the off-gas due to their gaseous precursors were ^{89}Sr, ^{137}Cs, ^{91}Y, and ^{140}Ba. Newer designs, as in the case of the TMSR-LF1, call for a more precise sparging system. For this work any simulation which includes sparging is modelled as a continuous process where the sparged gases are removed at a constant rate rather than in a batch process.

A portion of the circulating fuel salt (in the case of the TMSR ~10%) is continuously diverted from the primary loop into a stripping system (Chen et al., 2019). This system consists of a venturi bubble generator, Figure 5, which injects a stream of helium gas into the salt. These small bubbles of helium entrain the noble gasses krypton and xenon as well as tritium. The helium bubbles are then stripped from the fuel salt by a liquid-gas separator just downstream, a schematic of which can be seen in Figure 6. The spiral vein generated in the liquid-gas separator must be well tuned to create a pure column of helium that can be redirected to the off-gas stream without creating a fine mist of fuel salt. The sparging gas stream is then cleaned of xenon, krypton, and tritium by a three-stage cryogenic condensation system. The estimated efficiency for removal of xenon, krypton, and tritium is 70% for this combined system (Robertson, 1971). (For reference, the TMSR has a primary fuel salt flow rate of 2.24×10^{4} cm^3/s)

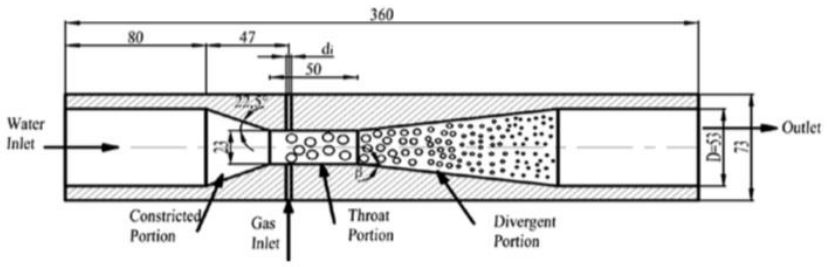

Figure 5. Schematic of a benchtop venturi bubble generator from (Li et al., 2017)

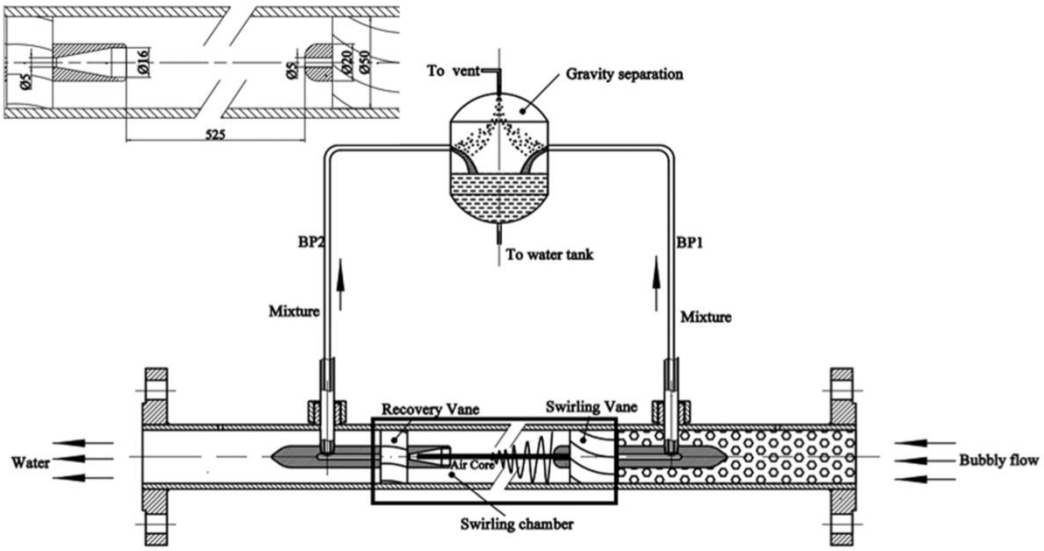

Figure 6. Schematic of a benchtop liquid-gas separator from (Yin et al., 2015)

1.1.2 Abatement and Holdup of Sparged Isotopes

Once gases and volatiles are removed from the fuel stream, either through sparging or other reprocessing methods, they then enter an abatement system. This system is key to ensuring that unnecessarily high levels of radioactivity are not introduced into the environment surrounding a facility. These methods, or the lack thereof, can have a significant impact on the near- and far-field concentration of gaseous, volatile, and non-volatile isotopes, as well as isotopes with gaseous or volatile precursors (Miley et al., 2017). In particular, the IMS relevant xenon isotopes are significantly impacted by abatement methods and timing. Releases of ^{133}Xe are of particular interest to the monitoring community since elevated ^{133}Xe backgrounds already exist worldwide and additional releases would only serve to compound the issue (Bowyer, 2020; Saey, 2009). Past work focused on medical isotope production facilities (MIPFs) proposed a ^{133}Xe emissions target of 5×10^9 Bq/d to maintain ^{133}Xe backgrounds at a sustainable level (Bowyer et al., 2013).

The MSRE provides the most detailed account of such an off-gas or cover gas abatement system (Robertson, 1965). Helium flowed through the pump bowl at a flow rate of 200 ft^3/day to extract the fission product gases from the reactor salt. The radioactive gas mixture was passed

through a series of pipes to provide a two-hour decay of the short-lived nuclides before being filtered through activated charcoal traps. The xenon was then held on the charcoal for a minimum of 90 days and the krypton was retained for 7.5 days. This hold-up time allowed the ^{85}Kr to decay to “insignificant” levels. At release the remaining krypton and xenon gasses were passed through one final filter, monitored for activity, and then diluted with 21,000 ft^3 of air while being dispersed out of a 100-ft tall vent stack.

Other portions of the MSRE system also vented to the stack including the fuel salt drain tanks, fuel pump shaft seal, graphite sampler, sample enricher, coolant salt pump seal, and coolant salt drain cell (Robertson, 1965). Similar to the first portion of the pump bowl line, gas lines coming from all of these system components had long piping sections to provide hold-up times of at least an hour to allow short-lived fission products to decay before making their way to the activated charcoal bed. The coolant salt loop cover gas differed in that it bypassed the charcoal beds and went straight to being monitored, filtered once, and discharged. The operating limits for radioactive gasses from all subsystems of the MSRE, averaged over a 12-month period, were set at 0.02294 MBq/sec of iodine, 2.923 MBq/sec of noble gases, and 1.332 MBq/sec of all other fission products (Guymon and Haubenreich, 1969).

2.0 Reactor Simulations

In order to examine the signatures of MSRs and assess their potential impact on the IMS, simulations were performed to understand what isotopes might be produced in MSRs and in what quantities. Four MSR designs were chosen, one from each category listed in Table 2, and are described in Table 3. Additionally, since the TMSR-LF1 reactor is likely to be the first MSR design to come online in the near-future, two fuel variations of the TMSR-LF1 reactor were simulated.

Additional simulations were also performed on three traditional reactors, a General Electric (GE) Boiling Water Rector (BWR), a Westinghouse Pressurized Water Reactor (PWR) and a High-Power Channel-Type Reactor (RBMK). All three traditional reactor designs utilize solid uranium dioxide fuel and are cooled with light water. The BWR and PWR are also light water moderated while the RBMK utilizes graphite as a moderator.

2.1 Molten Salt Reactors

Simulations performed to predict the production of fission and activation products were conducted on models mentioned in Section 1.1 using the COUPLE and ORIGEN modules of the SCALE 6.2.4 software package (Rearden and Jessee, 2018). The COUPLE module was used to calculate a set of flux-weighted, single-group cross-section libraries from user-provided neutron flux spectra (described below). Design specific neutron flux spectra were used for each reactor type. In order to simplify the simulation setup, only the neutron spectrum at reactor equilibrium was used.

The Oak Ridge Isotope Generation (ORIGEN) module of SCALE was used to calculate time-dependent activation and fission product production in the various target materials (fuel salt, cover gas). ORIGEN accounted for radioactive decay, particle-induced reactions, and the ingrowth of decay products and utilized the single group cross-sections from COUPLE to calculate production rates of fission and activation products (Rearden and Jessee, 2018). For these simulations, a 200-neutron fine-group library based on ENDF/B-VII.1 was used for the cross-section calculations. One isotope of interest, ^{196m}Au, was not available in the standard libraries and will not be reported here.

2.1.1 Simulation parameters

Where possible all parameters are derived from the literature, and in cases where literature values were not available the operating assumptions are listed. Table 3 lists the composition of fuel salt used for each reactor simulation. Only the salt circulating in the primary loop, the fuel salt, was considered in this simulation suite. The fuel salt volume and density were used to convert molar percentages to mass for use in the ORIGEN simulations.

Table 4 lists the specific actinide mixtures used in the MOSART and DFR reactors. For the case of the DFR, no fuel salt volume could be found in the literature, so the MSBR volume was chosen as a representative case.

Table 3. Fuel salt parameters used in the isotope production simulations of each listed reactor type.

Reactor	Fuel Salt Composition [mol %]	Fuel Salt Volume [m^3]	Fuel Salt Density [g/cc]	Neutron Flux in Fuel [n/cm^2 sec]	Power [MWth]	Reference
TMSR-LF1	65.39% ^{7}LiF (99.95% enriched ^{7}Li) 28.34% BeF_2 4.72% ZrF_4 1.55% UF_4 (19.75% enriched U)	2	2.307	1.3×10^{13}	2	(Liu et al., 2020; Zhou et al., 2020a)
TMSR-LF1 thorium	65.64% ^{7}LiF (99.95% enriched ^{7}Li) 27.27% BeF_2 4.54% ZrF_4 1.55% UF_4 (19.75% enriched U) 1% ThF_4	2	2.412	1.3×10^{13}	2	(Liu et al., 2020; Zhou et al., 2020a)
MSBR	71.75% ^{7}LiF (99.95% enriched ^{7}Li) 16% BeF_2 12% ThF_4 0.25% UF_4	48.7	3.35	1.5×10^{15}	2250	(Robertson, 1971; Rykhlevskii et al., 2019)
MOSART	15% ^{7}LiF (99.99% enriched ^{7}Li) 27% BeF_2 58% NaF 0.7% ActinideF_3†	40.4	2.163	1×10^{15}	2400	(Ignatiev et al., 2007; Sheu et al., 2013)
DFR	75% ^{37}Cl 19.586% ^{238}U 5.414% Mixed Pu†	48.7*	3.532	1.5×10^{15}*	3000	(Huke et al., 2015; Wang and Macian-Juan, 2018)

*No value found in the literature. Uses the value for the MSBR from (Rykhlevskii et al., 2019).
†Actinide breakdown listed in

Table 4

Table 4. Breakdown of the actinide composition for the MOSART reactor and the Pu mixture for the DFR. The weight percentages are for 100% of the actinides. The actinide contribution to the fuel salt is listed in Table 3.

Reactor	Actinide	Weight % of Actinides
MOSART	^{237}Np	5
	^{238}Pu	3
	^{239}Pu	50
	^{240}Pu	25
	^{241}Pu	7
	^{242}Pu	4
	^{241}Am	4
	^{243}Am	2
DFR	^{238}Pu	2.07
	^{239}Pu	58.11
	^{240}Pu	24.90
	^{241}Pu	8.68
	^{242}Pu	6.23

As part of each reactor simulation, the COUPLE module of SCALE was used to create a reactor specific cross-section library by calculating the flux-weighted average cross-sections for a user provided neutron flux profile. The production of various isotopes in the reactor is heavily dependent on the neutron spectrum and the location of the target nuclide in the core (Liu et al., 2020). For that reason, reactor specific spectra were used for each reactor type. The normalized neutron flux profile for each reactor type is shown in Figure 7. The following sources were used for the neutron fluxes: TMSR (Zhou et al., 2020a), MSBR (Rykhlevskii et al., 2019), MOSART (Sheu et al., 2013), DFR (Wang and Macian-Juan, 2018). In cases where multiple flux profiles were available the equilibrium case in the primary loop was always chosen.

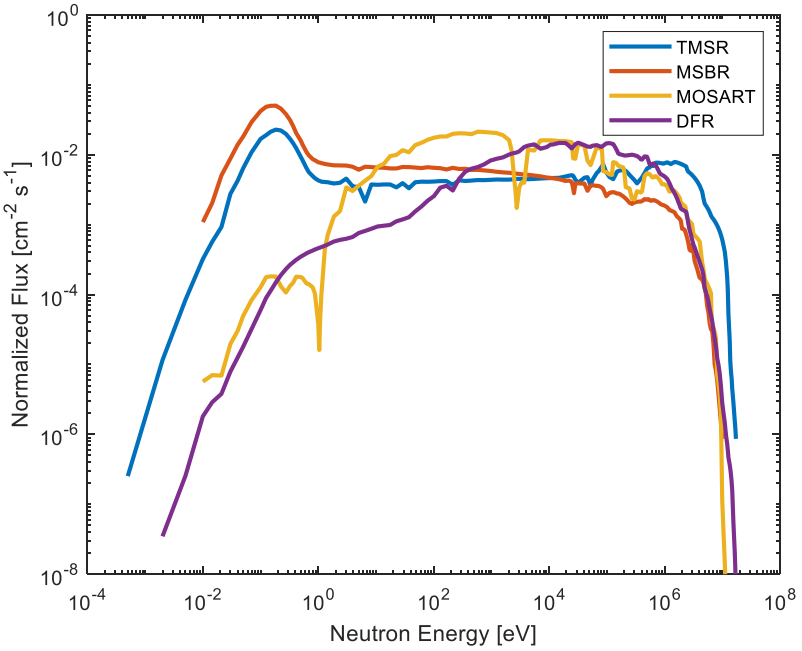

Figure 7. Normalized neutron flux spectra used to create the flux-weighted single group cross-sections in COUPLE.

The total neutron flux used for each reactor is shown in Table 5 along with the expected thermal power output of each reactor. No literature value for the neutron flux in the primary loop was found for the DFR, so the value for the MSBR was chosen as a representative case since it is the most heavily documented design among those considered here.

Table 5. Neutron flux expected total power output, and the associated references for each reactor type.

Reactor	Neutron Flux in Fuel [n/cm^2 sec]	Power [MWth]	Reference
TMSR-LF1	1.30×10^{13}	2	(Zhou et al., 2020a)
MSBR	1.50×10^{15}	2250	(Rykhlevskii et al., 2019)
MOSART	1.00×10^{15}	2400	(Sheu et al., 2013)
DFR	1.50×10^{15}*	3000	(Huke et al., 2015)

*No value found in the literature. Uses the value for the MSBR from (Rykhlevskii et al., 2019).

Each reactor was assumed to operate continuously for 300 days to match the expected operational cycle of the TMSR reactor (Zhou et al., 2020a).

2.1.2 Continuous Reprocessing and Refueling

In some cases, the expected reactor operational cycle includes the continuous removal of some fission products and the addition of actinides. While this removal and refueling process might be expected to happen in a batch process, for the ease of simulation the processes were all assumed to happen continuously at various rates. For this work two reactor designs were assumed to have continuous reprocessing, the MSBR and MOSART. DFR will likely also have continuous reprocessing but was not considered here due to a lack of supporting literature. The TMSR-LF1 reactor was assumed to be a research reactor that will not have online reprocessing, at least not initially.

MSBR

The removal rates for various elements from the MSBR fuel salt are listed in **Error! Reference source not found.**. Refueling (addition of ^{232}Th) was also assumed to occur continuously at a rate of 3.78×10^{-2} s^{-1}.

MOSART

The removal rates for various elements from the MOSART fuel salt are listed in

Table 6 and the refueling rates are listed in Table 7. The refueling rates are derived from the assumption that 24.4 metric tons of actinides will be loaded into the reactor during a 30 year lifetime including the startup load of 3.4 metric tons (Sheu et al., 2013). The actinide distribution is assumed to be consistent throughout the lifetime of the reactor and matches that listed in (Sheu et al., 2013).

Table 6. Removal rates for various elements from the MOSART fuel salt. Calculated from (Rykhlevskii et al., 2019; Sheu et al., 2013)

	Elements	Removal Rate [1/s]
MSBR		
Group A1	Y, La, Ce, Pr, Nd, Pm, Sm, Gd	2.32×10^{-7}
	Eu	2.32×10^{-8}
Group B1	Se, Nb, Mo, Tc, Ru, Rh, Pd, Ag, Sb, Te	5.00×10^{-2}
Group C1	Zr, Cd, In, Sn	5.79×10^{-8}
Group D1	Kr, Xe	5.00×10^{-2}
Group E1	Br, I	5.00×10^{-2}
Group F1	Pa	3.86×10^{-6}
MOSART		
Group A2	Ag, As, Cd, Ga, Ge, In, Mo, Nb, Pd, Rh, Ru, Sb, Se, Sn, Tc, Te, Zn	5.00×10^{-2}
Group B2	He, Kr, Xe	5.00×10^{-2}
Group C2	Ba, Ce, Cr, Cs, Dy, Er, Eu, Fe, Gd, Ho, I, La, Nd, Ni, Pm, Pr, Rb, Sm, Sr, Tb, Y, Zr	3.86×10^{-6}

Table 7. Feed rate for continuous refueling of the MOSART reactor.

Isotope	Feed Rate [g/sec]
^{237}Np	1.11×10^{-3}
^{238}Pu	6.65×10^{-4}
^{239}Pu	1.11×10^{-2}
^{240}Pu	5.54×10^{-3}
^{241}Pu	1.55×10^{-3}
^{242}Pu	8.87×10^{-4}
^{241}Am	8.87×10^{-4}
^{243}Am	4.44×10^{-4}

2.1.3 Sparging

As discussed above in Section 1.1.1, sparging of the fuel salt to remove fission gases such as xenon and krypton is an important component of MSR operations as it removes the strong neutron poison ^{135}Xe. The sparging rate of the noble gases is listed in

Table 6 for the MSBR and MOSART designs as it was considered to be part of continuous reprocessing. The TMSR-LF1 design, which was assumed not to use continuous reprocessing, was simulated to have a removal rate of xenon and krypton of 7.84×10^{-4} 1/s. This assumes a salt flow rate of 2.24×10^{4} cc/s, a 10% fuel diversion, and removal efficiency of 70% per cycle (Robertson, 1971; Zhou et al., 2020b).

2.2 Traditional Reactors

Three traditional NPP designs were simulated to provide a comparison against the MSRs described previously. The three designs chosen were the BWR, the PWR, and the graphite moderated high-power channel-type reactor (RBMK). These designs were chosen as they represent a large fraction (85%) of the commercial nuclear power reactors currently in operation around the globe (International Atomic Energy Agency, 2019).

The ORIGAMI module of SCALE was used to simulate the irradiation of one metric ton of uranium (MTU) in each reactor type for 300 days (Rearden and Jessee, 2018). This simulation set was simplified by assuming that no non-fuel elements are present and that the fuel is irradiated in a single 300-day pass. It was also assumed that the reactor contained fresh fuel that had not been previously irradiated. The reactor-specific details are provided in Table 8. After the 300-day irradiation cycle was complete in ORIGAMI the isotopic information was then passed to ORIGEN and the decay of the irradiated fuel was tracked for 1800 days after shutdown.

Table 8. Fuel type, moderator density, and power used in simulations of three traditional power reactors.

Reactor	Assembly Type	Fuel Enrichment [%]	Moderator Density [g/cm^3]	Power [MW/MTU]
BWR	GE 10x10-8	4	0.73	40
PWR	Westinghouse 17x17	4	0.7	40
RBMK	RBMK-1000	2.6	0.54	20

In order to calculate the total reactor inventory of radionuclides, each reactor was assumed to contain 100 MTU at startup. A comparison was made between the BWR radioxneon inventories calculated here to those for the Fukushima Daichi NPP (Bowyer et al., 2011). Accounting for the fact that the inventory at Fukushima Daichi included contributions from three operating reactors, the results of this work agree well, although this work consistently reports a higher inventory. This is likely due in part to the imprecise 100 MTU fuel load used here rather than the specific reactor inventories used in (Bowyer et al., 2011).

2.3 Activation Products

The unique neutronic, heat transfer, and physicochemical properties of FLiBe (Li_2BeF_4) salt make it one of the promising fuel salts suitable for a MSR (Dolan, 2017; Ying et al., 2019). Although the salt possesses inherently low activation characteristics, the activation products and their signatures can be notably different from BWRs and PWRs (Klix et al., 2005; Ying et al., 2019). Furthermore, any impurities that accompany the salt and corrosion products, produced from interactions of the molten salt with structural materials, can significantly alter the activation products' signatures. As an example, the TMSR-LF1 reactor model was used and the activation products' signatures were observed during and post full power operation of the reactor. The

impurities and corrosion concentrations considered in this study were taken from previous studies (Klix et al., 2005; Ying et al., 2019). The motive was to not only understand the activation products that are generated from corrosion products/impurities but also focusing on those that are relevant to IMS (Burnett et al., 2019).

To determine time-dependent activation products' signatures, two independent simulations were performed using ORIGEN. The first simulation studied the ingrowth of activation products as the reactor operates and the second simulation investigated their decay after the reactor is shut down (or the salt is removed from the reactor vessel); the irradiation time in the second simulation was set to 100 days (the same duration used by (Ying et al., 2019)) and the decay was observed thereafter.

3.0 Results

3.1 Xenon Release Magnitude

The magnitude of xenon releases is a major factor when determining the impact of MSRs on the IMS (Table 9). The xenon removal rate in 1/s (shown in

Table 6) was used as the fraction of xenon released at a single point in time during the equilibrium phase of the reactor cycle. This was assumed to be equivalent to be the amount of xenon released over a one second period. In order to convert to a release rate of Bq/d, the one second release was then multiplied by 86400, or the number of seconds in one day. The removed xenon fraction was then allowed to decay in order to simulate the hold-up of xenon in some retention system like that described in Section 1.1.1, and the approximate number of days necessary to reach a threshold of 5×10^9 Bq/d of ^{133}Xe was determined.

Table 9. Calculated xenon emissions from MSR's with no xenon abatement.

Reactor	^{131m}Xe [Bq/d]	^{133}Xe [Bq/d]	^{133m}Xe [Bq/d]	^{135}Xe [Bq/d]
MSBR	1.83×10^{13}	7.72×10^{16}	1.51×10^{16}	6.45×10^{18}
MOSART	8.78×10^{12}	6.78×10^{16}	9.41×10^{15}	5.93×10^{18}
TMSR-LF1	2.57×10^{12}	1.20×10^{15}	8.27×10^{13}	1.38×10^{16}
TMSR-LF1-thorium	2.45×10^{12}	1.14×10^{15}	8.13×10^{13}	1.31×10^{16}

3.2 Radioxenon signatures of molten salt reactors

In Figure 8 a ratio plot of the four primary radioxenon isotopes of interest is shown for an entire reactor cycle from startup, through three-hundred days of continuous operation, shutdown, and decay of the fuel salt after shutdown. The case shown in Figure 8 assumes that there is no reprocessing, refueling, or sparging of the fuel. Also shown is the discrimination line proposed to distinguish between nuclear explosives and reactor operations based on isotopic ratios taken from direct measurements of four xenon isotopes or inferred based on the minimum detectable concentration of these four isotopes (Kalinowski et al., 2010), where signatures on the left of the line are generally considered to come from civilian sources and signatures to the right of the line may come from a nuclear explosion.

If the signatures are separated out by phase as shown in Figure 9 it becomes apparent that the greatest impact to the IMS network is likely to come during reactor startup. This result mirrors that reported in (Kalinowski et al., 2010) for light water reactors (LWRs).

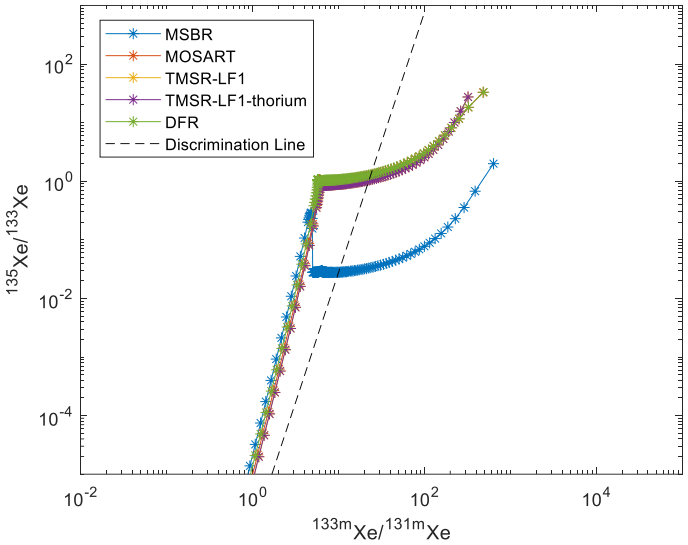

Figure 8. Multi-isotope ratio plot for radioxenon produced by five molten salt reactor types. These plots represent operation without sparging, reprocessing, or refueling.

If sparging, reprocessing and refueling are omitted, which may be true for small modular MSRs, Figure 9a shows that in the first 60 days of operation xenon isotopic ratios ($^{135}Xe/^{133}Xe$ and $^{133m}Xe/^{131m}Xe$) are consistent with those seen in a nuclear explosion. Within the operation range of 60 days – 3 years, these ratios are representative of civilian operations.

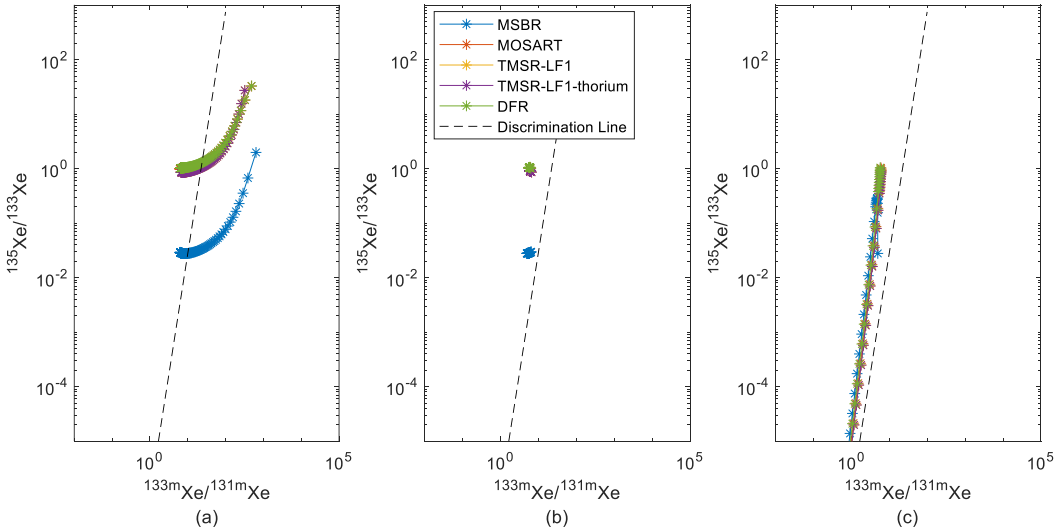

Figure 9. 4-isotope xenon ratio plot for (a) the first 60 days of operation after reactor startup, (b) reactor operation from 60 days to 3 years of continuous operation, and (c) decay of fuel salt following shutdown after 3 years of continuous operation. This plot represents operation without sparging, reprocessing, or refueling.

However, if continuous reprocessing and refueling are considered, like the cases shown in Figure 10 for MOSART and MSBR, then the impact on IMS stations may be significantly greater since the reactor emissions remain in the traditional nuclear explosion region for the entire

operational life of the reactor. This is primarily due to the removal of the xenon precursors Sb, Te, and I rather than the removal of the xenon itself. In particular, the removal of Te has the most significant impact on the xenon signature, far greater than I or Sb. Reactors of this type would have to be monitored closely or other methodologies developed to verify their emissions.

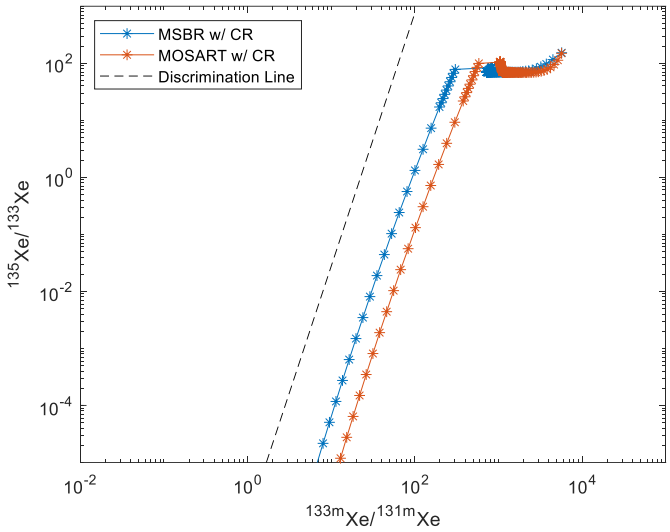

Figure 10. 4-isotope xenon ratio plot for operation of two molten salt reactor types from startup, through 3 years of continuous operation, and decay of duel salt after shutdown. Both reactor simulations include continuous reprocessing and refueling.

In Figure 11 the signatures produced by the TMSR-LF1 reactor are shown with and without continuous removal of xenon and krypton. While the signatures do vary between the two cases due to a restricted build-up of longer-lived isotopes such as ^{133}Xe and ^{131m}Xe, in both cases the resulting signatures fall on the civilian source side of the discrimination line.

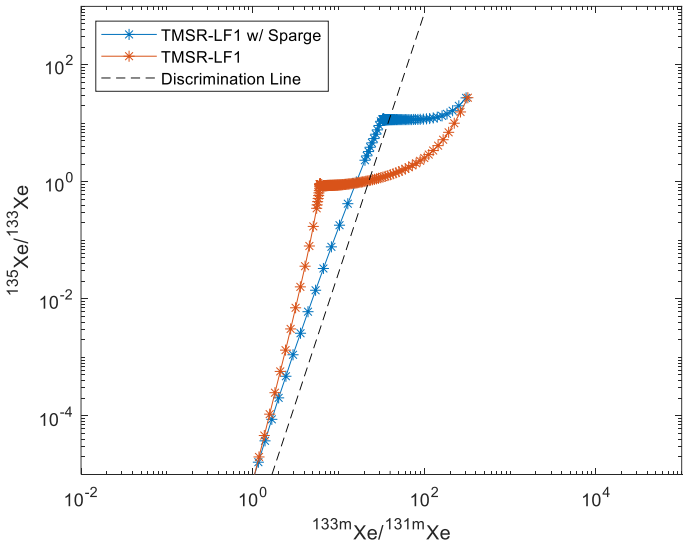

Figure 11. 4-isotope xenon ratio plot for operation of the TMSR-LF1 reactor with and without sparging (removal of gaseous fission products).

3.3 Radioiodine signatures of molten salt reactors

Like radioxenon, isotope ratio plots of radioiodine (^{135}I, ^{133}I, ^{131}I) may also be useful for source discrimination of radioactive releases. In Figure 12, an isotopic ratio plot is shown for three radioiodine isotopes ^{131}I, ^{133}I, and ^{135}I produced throughout the life cycle of four MSR's assuming no reprocessing, refueling, or sparging of the fuel. Like in the xenon plots, a discrimination line has been proposed which may aid in the discrimination of civilian and weapon signatures (Kalinowski et al., 2014). Similar to those for xenon, iodine isotopic ratios resembling a nuclear explosion are only observed during reactor start-up (0 – 60 days).

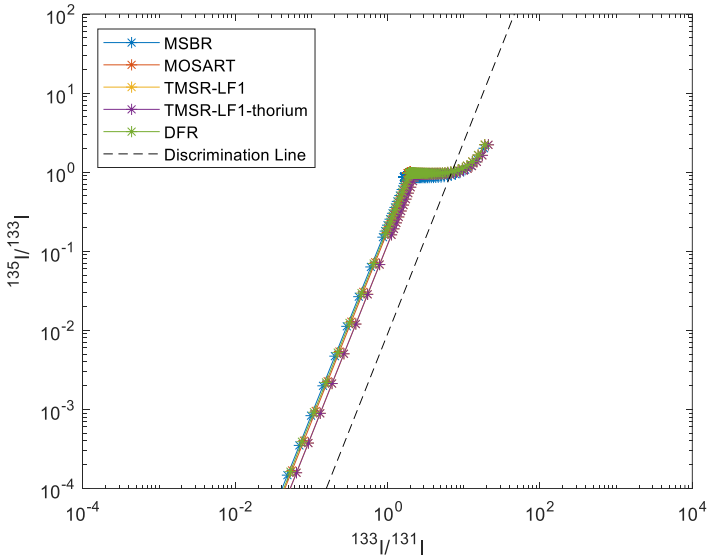

Figure 12. Multi-isotope plot of radioiodine signatures from MSR's without continuous reprocessing or refueling.

However, as in the case of the xenon signatures, continuous reprocessing of the fuel salt shifts the MSR signatures below the discrimination line and into the region generally associated with nuclear weapon explosions as shown in Figure 13. This is due primarily to the removal of iodine and its precursors Sb and Te. However, in contrast to the xenon signatures, ceasing removal of any one of these elements is sufficient to shift the iodine signatures to the civilian side of the discrimination line. Sparging has no impact on the radioiodine signatures since none of its precursors are gases which would be eliminated during this process.

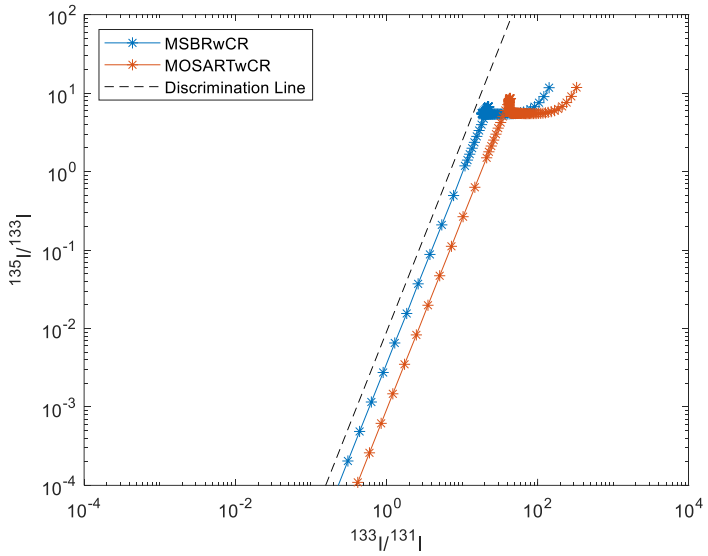

Figure 13. Multi-isotope plot of radioiodine signatures from MSR's with continuous reprocessing and refueling.

4.0 Activation Product Evolution

As discussed in section 2.3, two independent simulations were performed for both pure and impure (with corrosion products) FLiBe for key activation products. While a complete list of activation products that are relevant to IMS is given in (Burnett et al., 2019), Table 10 presents the activation products whose signatures were altered when impurities were considered. As already mentioned in section 2.3, the TMSR-LF1 reactor model was used in these simulations; the activities reported in Figure 14 and Figure 15 are for fuel composition/volume given in Table 3 for TMSR-LF1 reactor.

Figure 14 shows the ingrowth and decay of activation products that develop due to added impurities/corrosion products. Nuclear reactions that result in ingrowth of these isotopes are given in Table 10. The signatures of ^{16}N, ^{20}F, and ^{19}O from pure and impure FLiBe were unaltered as these isotopes are directly produced from activation of FLiBe salt (and not by the impurities/corrosion products); hence these isotopes are not shown in Figure 14 or **Error! Reference source not found.**.

As seen in Figure 14(a), in general the change of activity with time follows the expected trend of monotonic growth with time followed by saturation proportional to respective half-life (Zhou et al., 2020a). The saturation time for the isotopes shown in Figure 14(a) is ~10-11 times that of their half-life. For initial ~28 hours, the activity is dominated by ^{24}Na, which develops due to irradiation of Na, Mg, and Al impurities in the salt (see Table 11). After this time, ^{51}Cr, developed from irradiation of Fe and Cr corrosion products, has the highest activity. It is interesting to note that two key activation products that are relevant to IMS, ^{42}K and ^{65}Zn, had negligible activities for short periods. However, the activity of these two isotopes increased monotonically with time and reached 10 Bq in approximately 1.1 and 2.1 years, respectively. For the highest time considered in the simulation (10^9 sec since startup) their activity were approximately 5.1×10^2 and 8.5×10^4 Bq, respectively.
To investigate the origin of ^{42}K and ^{65}Zn, several independent simulations were performed and compared by including the impurities one by one. It was observed that ^{42}K and ^{65}Zn were produced from titanium and nickel, respectively. One of the possible routes for ingrowth of ^{42}K is via following reactions occurring in succession: $^{46}\mathrm{Ti}(n,p)^{46}\mathrm{Sc}$, $^{46}\mathrm{Sc}(n,\alpha)^{43}\mathrm{K}$, and $^{43}\mathrm{K}(n,2n)^{42}\mathrm{K}$ (or $^{43}\mathrm{K}(n,\gamma)^{44}\mathrm{K}$, and $^{44}\mathrm{K}(n,3n)^{42}\mathrm{K}$). It is envisaged that ^{65}Zn is produced through $^{62}\mathrm{Ni}(\alpha,n)^{65}\mathrm{Zn}$ reactions, with alpha particles produced via (α,n) reactions in the FLiBe salt. Considering Figure 14(b), the decay activity is initially dominated by ^{51}Cr (t <136 days after shutdown) while the later activity has major contributions from ^{60}Co. Although the initial activities of ^{58}Co and ^{60}Co are similar, ^{58}Co dies off earlier due to its relatively short half-life (70.9 days vs 5.27 years). As an example, the activity of ^{58}Co and ^{60}Co reaches 1 Bq in 7.2 and 194 years, respectively (in accordance with the ratio of their half-life). This argument is also valid for ^{59}Fe and ^{54}Mn.

Table 10. Activation products following salt irradiation. Properties of activation products that are relevant to IMS and develop due to impurities/corrosion products are also given (National Institute of Standards and Technology, 2020; National Nuclear Data Center, 2016).

Nuclide name	Half-life	Reaction
FLiBe salt:		
^{16}N	7.13 s	$^{19}\mathrm{F}(\mathrm{n},\alpha)^{16}\mathrm{N}$
^{20}F	11.0 s	$^{19}\mathrm{F}(\mathrm{n},\gamma)^{20}\mathrm{F}$

^{19}O	26.9 s	$^{19}F(n,p)^{19}O$
Corrosion products/impurities *Relevant to IMS:*		
^{57}Co	271.7 d	$^{58}Ni(n,2n)^{57}Co$ $^{59}Co(n,3n)^{57}Co$
^{58}Co	70.9 d	$^{58}Ni(n,p)^{58}Co$ $^{59}Co(n,2n)^{58}Co$ $^{60}Ni(n,t)^{58}Co$
^{60}Co	5.27 y	$^{59}Co(n,\gamma)^{60}Co$ $^{60}Ni(n,p)^{60}Co$ $^{62}Ni(n,t)^{60}Co$
^{51}Cr	27.7 d	$^{50}Cr(n,\gamma)^{51}Cr$ $^{52}Cr(n,2n)^{51}Cr$ $^{53}Cr(n,3n)^{51}Cr$ $^{54}Fe(n,\alpha)^{51}Cr$
^{59}Fe	44.5 d	$^{58}Fe(n,\gamma)^{59}Fe$ $^{59}Co(n,p)^{59}Fe$ $^{62}Ni(n,\alpha)^{59}Fe$
^{54}Mn	312.2 d	$^{54}Fe(n,p)^{54}Mn$ $^{56}Fe(n,t)^{54}Mn$ $^{55}Mn(n,2n)^{54}Mn$
^{24}Na	15.0 h	$^{23}Na(n,\gamma)^{24}Na$ $^{24}Mg(n,p)\ ^{24}Na$ $^{26}Mg(n,t)\ ^{24}Na$ $^{27}Al(n,\alpha)\ ^{24}Na$
^{46}Sc	83.8 d	$^{46}Ti(n,p)^{46}Sc$ $^{48}Ti(n,t)^{46}Sc$
^{47}Sc	3.3 d	$^{47}Ti(n,p)^{47}Sc$ $^{49}Ti(n,t)^{47}Sc$ $^{50}Ti(n,\alpha)^{47}Sc$ $^{50}V(n,\alpha)^{47}Sc$
Other (Not IMS relevant):		
^{65}Ni	2.5 h	$^{64}Ni(n,\gamma)^{65}Ni$
^{56}Mn	2.6 h	$^{55}Mn(n,\gamma)^{56}Mn$ $^{56}Fe(n,p)^{56}Mn$ $^{58}Fe(n,t)^{56}Mn$ $^{59}Co(n,\alpha)^{56}Mn$
^{55}Fe	2.7 y	$^{54}Fe(n,\gamma)^{55}Fe$ $^{56}Fe(n,2n)^{55}Fe$ $^{57}Fe(n,3n)^{55}Fe$ $^{58}Ni(n,\alpha)^{55}Fe$
^{63}Ni	101.2 y	$^{62}Ni(n,\gamma)^{63}Ni$ $^{64}Ni(n,2n)^{63}Ni$
^{59}Ni	7.6×10^{4} y	$^{58}Ni(n,\gamma)^{59}Ni$ $^{60}Ni(n,2n)^{59}Ni$ $^{61}Ni(n,3n)^{59}Ni$

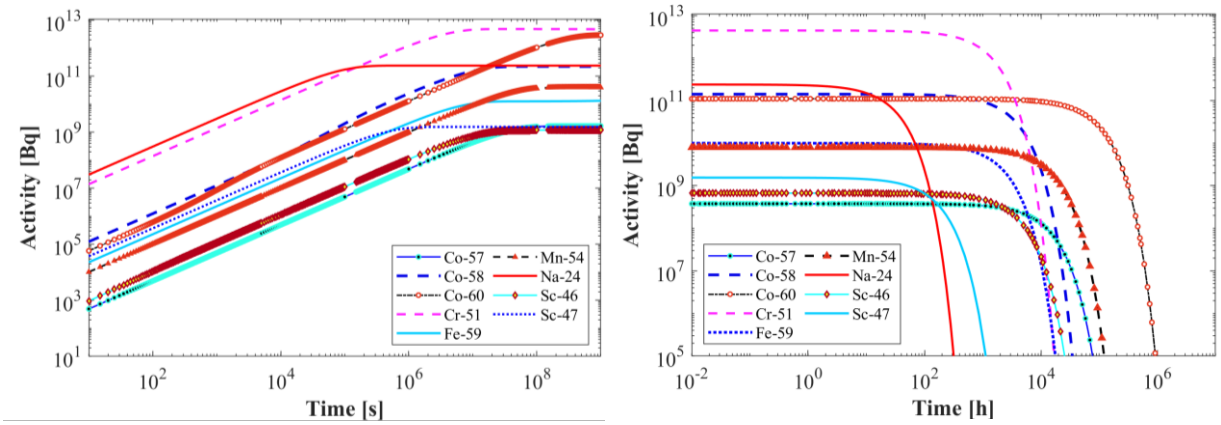

(a) (b)

Figure 14. Activity variation of activation products that are relevant to IMS during reactor (a) operation, and (b) cooling after 100 days of irradiation/operation.

Similar ingrowth nature also exists for other activation products that are not relevant to the IMS (see **Error! Reference source not found.**(a)). As can be seen in **Error! Reference source not found.**(a), the activity is primarily dominated by ^{56}Mn which develops from irradiation of Fe, Co, and Mn impurities. Nickel isotopes—^{59}Ni and ^{63}Ni—do not saturate in the time considered (5-10^{9} sec) due to their relatively long half-life (7.6×10^{4} and 100 years, respectively). On comparison with previous published results (Zhou et al., 2020a), the saturation activities of the isotopes in this work are higher. . This is because (Zhou et al., 2020a) considered the salt in the secondary (coolant) loop while this work only examined salt in the primary (fuel) loop. The decay of these activation products after 100 days of irradiation is shown in **Error! Reference source not found.**(b). Manganese-56 dies off (<10 Bq) in ~100 hours, with ^{59}Ni and ^{63}Ni surviving even after 114 years.

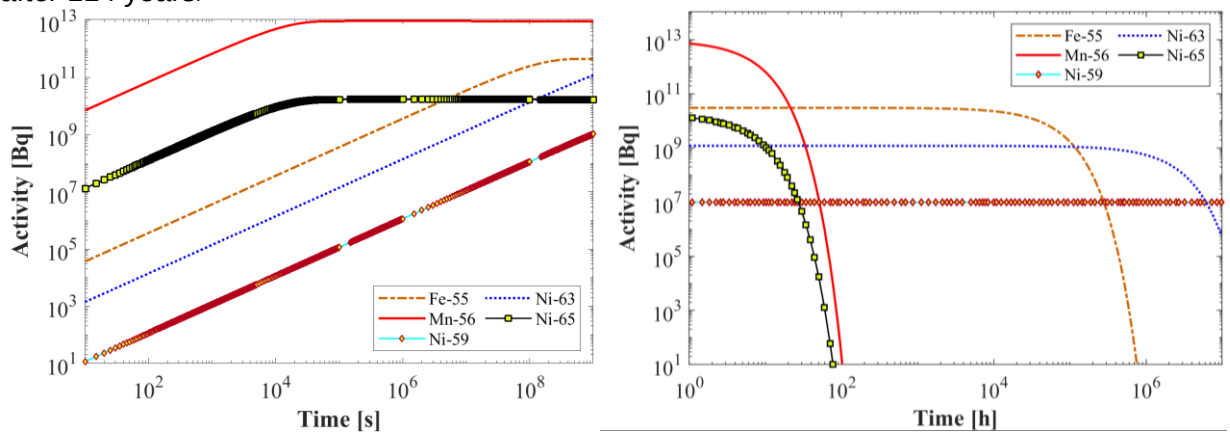

(a) (b)

Figure 15. Variation of activation products' activity during reactor (a) operation, and (b) cooling after 100 days of irradiation.

5.0 Signature Comparisons

Seventeen key IMS relevant radionuclides for all four MSRs are compared to the conventional reactor types BWR, PWR, and RBMK in **Error! Reference source not found.**-**Error! Reference source not found.**. For the complete list of IMS relevant radionuclides, minus ^{196m}Au, see Appendix A.

Comparing the results in Table 11, the sealed reactor cases, the MSBR and DFR have a significantly higher ^{134}Cs and ^{136}Cs inventory and, in the case of the MSBR, a relatively low ^{103}Ru inventory as a fraction of the total activity in the reactor. This is likely due to the variations in fission yield for these isotopes between the standard ^{235}U and ^{238}U and the fission yield of the ^{232}Th and ^{233}U used in the MSBR. In the case of ^{103}Ru the fission yield differences are particularly dramatic between the low-Z fissionable isotopes like ^{232}Th and ^{233}U (used in the MSBR) and the high-Z fissionable isotopes such as the TRU/MOX fuel used in the MOSART and DFR reactors where ^{103}Ru contributions are up to an order of magnitude higher. The ^{103}Ru case is one of the most dramatic, but variations in fission yields are apparent across the suite of isotopes. Another isotope with a dramatically different production rate is ^{135}Xe, which contributes a significantly lower fraction of the total reactor activity in the MSBR than in other reactor designs. In most cases, ^{135}Xe contributes nearly 1% of the total activity in the reactor at 180 days, but in the ^{232}Th-fueled MSBR the contribution is only 0.01%.

In the case of the TMSR-LF1, the reactor inventories are significantly lower than in all other cases. This is due primarily to the smaller size of the reactor (2 MWth). Little difference is observed in the signatures when the thorium fuel load is considered rather than uranium; however, unlike the MSBR case where the thorium was 12% of the total fuel the TMSR-LF1 thorium case only consists of 1% thorium fuel.

Error! Reference source not found. presents the reactor inventory (in Bq) for the MSBR and MOSART when continuous reprocessing and refueling are anticipated. Here, the 17 key relevant radionuclides are either within the range of those of the corresponding BWR, PWR and RBMK reactors or lower in the case of the xenon isotopes, ^{103}Ru, ^{132}Te, ^{134}Cs and ^{95}Nb and ^{99}Mo. Even at these lower activities the impact could be worse on IMS since the releases of isotopes including xenon would be continuous if no abatement is employed.

Error! Reference source not found. representing TMSR-LF and TMSR-LF1 thorium with continuous sparging under continuous operations, shows a similar trend as that seen for MSBR and MOSART reactor types under continuous operations and continuous reprocessing.

Table 11. Reactor inventory (in Bq) of 17 key relevant radionuclides after 180 days of continuous operation with no reprocessing or refueling as calculated in this work.

	Activity [Bq]							
Isotope	MSBR	MOSART	DFR	TMSR-LF1	TMSR-LF1 thorium	BWR	PWR	RBMK
^{131m}Xe	3.34E+17	2.23E+16	2.10E+17	4.39E+13	4.18E+13	4.16E+16	4.17E+16	2.05E+16
^{133}Xe	5.35E+19	3.82E+18	3.59E+19	8.85E+15	8.41E+15	8.39E+18	8.38E+18	4.21E+18
^{133m}Xe	1.86E+18	1.17E+17	1.10E+18	2.43E+14	2.31E+14	2.47E+17	2.47E+17	1.23E+17
^{135}Xe	1.58E+18	4.03E+18	3.83E+19	8.08E+15	7.69E+15	2.27E+18	2.42E+18	1.26E+18
^{103}Ru	1.37E+19	3.93E+18	3.50E+19	4.14E+15	3.93E+15	4.44E+18	4.46E+18	2.11E+18
^{131}I	3.43E+19	2.13E+18	1.96E+19	4.05E+15	3.85E+15	3.82E+18	3.82E+18	1.89E+18
^{132}Te	4.62E+19	2.89E+18	2.70E+19	6.02E+15	5.72E+15	5.58E+18	5.58E+18	2.77E+18
^{133}I	5.89E+19	4.02E+18	3.78E+19	9.35E+15	8.89E+15	8.30E+18	8.29E+18	4.17E+18
^{134}Cs	9.24E+17	4.94E+16	1.34E+17	1.01E+12	9.56E+11	2.78E+16	2.94E+16	6.34E+15
^{136}Cs	1.03E+18	2.54E+17	8.82E+17	9.81E+12	9.45E+12	3.57E+16	3.87E+16	1.27E+16
^{137}Cs	6.12E+17	4.63E+16	3.77E+17	9.75E+13	9.26E+13	8.78E+16	8.77E+16	4.41E+16
^{140}Ba	6.10E+19	3.24E+18	2.99E+19	8.65E+15	8.23E+15	7.55E+18	7.53E+18	3.82E+18
^{143}Ce	5.88E+19	2.62E+18	2.46E+19	8.27E+15	7.87E+15	7.01E+18	6.97E+18	3.58E+18
^{95}Nb	3.52E+19	1.95E+18	1.64E+19	6.59E+15	6.26E+15	5.63E+18	5.62E+18	2.87E+18
^{95}Zr	4.70E+19	2.38E+18	2.03E+19	7.86E+15	7.46E+15	6.67E+18	6.65E+18	3.40E+18
^{97}Zr	5.44E+19	3.03E+18	2.84E+19	8.45E+15	8.02E+15	7.29E+18	7.27E+18	3.69E+18
^{99}Mo	4.94E+19	3.61E+18	3.37E+19	8.52E+15	8.09E+15	7.64E+18	7.62E+18	3.83E+18

Table 12. MSBR and MOSART reactor inventory of 17 key relevant radionuclides after 180 days of continuous operation with continuous reprocessing and refueling as calculated in this work. Comparison BWR, PWR and RBMK inventories after continuous operation for 180 days.

	Activity [Bq]				
Isotope	MSBR	MOSART	BWR	PWR	RBMK
^{131m}Xe	5.75E+09	2.28E+09	4.16E+16	4.17E+16	2.05E+16
^{133}Xe	2.33E+13	1.78E+13	8.39E+18	8.38E+18	4.21E+18
^{133m}Xe	4.61E+12	2.48E+12	2.47E+17	2.47E+17	1.23E+17
^{135}Xe	1.85E+15	1.42E+15	2.27E+18	2.42E+18	1.26E+18
^{103}Ru	3.29E+11	8.01E+11	4.44E+18	4.46E+18	2.11E+18
^{131}I	3.67E+16	1.40E+16	3.82E+18	3.82E+18	1.89E+18
^{132}Te	1.97E+14	8.24E+13	5.58E+18	5.58E+18	2.77E+18
^{133}I	7.69E+17	5.93E+17	8.30E+18	8.29E+18	4.17E+18
^{134}Cs	7.33E+13	4.41E+13	2.78E+16	2.94E+16	6.34E+15
^{136}Cs	1.11E+17	3.89E+16	3.57E+16	3.87E+16	1.27E+16
^{137}Cs	3.49E+16	5.32E+15	8.78E+16	8.77E+16	4.41E+16
^{140}Ba	7.04E+18	3.18E+18	7.55E+18	7.53E+18	3.82E+18
^{143}Ce	6.84E+18	3.38E+18	7.01E+18	6.97E+18	3.58E+18
^{95}Nb	3.51E+13	1.11E+13	5.63E+18	5.62E+18	2.87E+18
^{95}Zr	7.73E+18	2.45E+18	6.67E+18	6.65E+18	3.40E+18
^{97}Zr	6.55E+18	3.92E+18	7.29E+18	7.27E+18	3.69E+18
^{99}Mo	1.12E+14	8.53E+13	7.64E+18	7.62E+18	3.83E+18

Table 13. Reactor inventory of 17 key relevant radionuclides after 180 days of continuous operation with continuous sparging of the fuel salt as calculated in this work.

	Activity [Bq]				
Isotope	TMSR-LF1	TMSR-LF1 thorium	BWR	PWR	RBMK
^{131m}Xe	3.80E+10	3.61E+10	4.16E+16	4.17E+16	2.05E+16
^{133}Xe	1.77E+13	1.68E+13	8.39E+18	8.38E+18	4.21E+18
^{133m}Xe	1.25E+12	1.19E+12	2.47E+17	2.47E+17	1.23E+17
^{135}Xe	2.16E+14	2.05E+14	2.27E+18	2.42E+18	1.26E+18
^{103}Ru	4.14E+15	3.93E+15	4.44E+18	4.46E+18	2.11E+18
^{131}I	4.05E+15	3.85E+15	3.82E+18	3.82E+18	1.89E+18
^{132}Te	6.02E+15	5.72E+15	5.58E+18	5.58E+18	2.77E+18
^{133}I	9.35E+15	8.89E+15	8.30E+18	8.29E+18	4.17E+18
^{134}Cs	4.69E+09	4.50E+09	2.78E+16	2.94E+16	6.34E+15
^{136}Cs	7.16E+12	6.93E+12	3.57E+16	3.87E+16	1.27E+16
^{137}Cs	7.77E+13	7.38E+13	8.78E+16	8.77E+16	4.41E+16
^{140}Ba	8.57E+15	8.15E+15	7.55E+18	7.53E+18	3.82E+18
^{143}Ce	8.27E+15	7.87E+15	7.01E+18	6.97E+18	3.58E+18
^{95}Nb	6.59E+15	6.26E+15	5.63E+18	5.62E+18	2.87E+18
^{95}Zr	7.86E+15	7.46E+15	6.67E+18	6.65E+18	3.40E+18
^{97}Zr	8.45E+15	8.02E+15	7.29E+18	7.27E+18	3.69E+18
^{99}Mo	8.52E+15	8.09E+15	7.64E+18	7.62E+18	3.83E+18

5.1 Radioxenon comparison

In Figure 16 the radioxenon isotope ratios are shown for NPPS and MSRs operating without refueling, reprocessing, or sparging. In this case, the signatures of the MSRs are similar to those of the traditional power reactors after a 60-day startup period and fall on the “civilian” side of the discrimination line. This may be indicative of how small-modular reactors work, however, most proposed MSR designs are expected to have some combination of processing steps. Even though the majority of the reactor’s life cycle is spent above the discrimination line, care should be taken during reactor startup since the signatures during this period may still fall below the discrimination line. The time necessary for the reactor signatures to evolve varies between reactor designs and ranges from 13 days for the DFR and MOSART to 25 days for the MSBR.

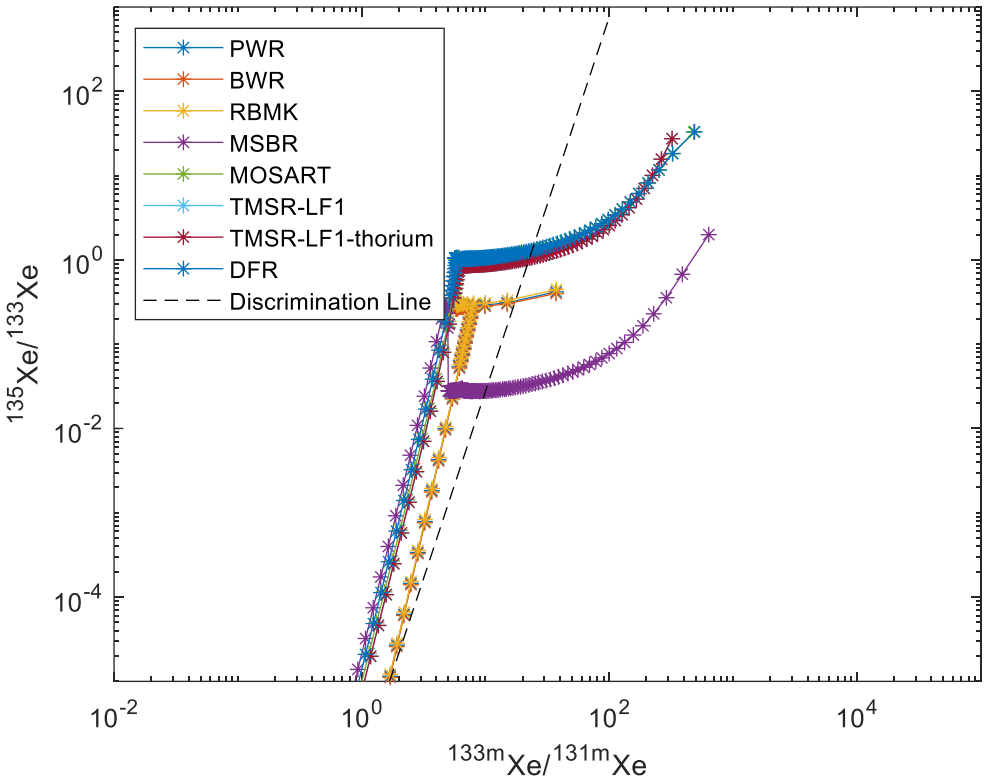

Figure 16. The four-isotope xenon ratio plots for various light water reactors for 300 days of operation. The decay phase assumes that xenon is released at 300 days of operation. Also shown are the xenon ratios for molten salt reactors without reprocessing, refueling, or sparging.

However, if continuous reprocessing and refueling are considered, like the cases shown in Figure 17 for MOSART and MSBR, then the impact on IMS stations may be significantly greater since the reactor emissions remain in the traditional nuclear explosion region for the entire operational life of the reactor. This is primarily due to the removal of the xenon precursors, Sb, Te, and I, rather than the removal of the xenon itself. In particular, the removal of Te has the most significant impact on the xenon signature, far greater than I or Sb. Reactors of this type would have to be monitored closely or other methodologies developed to verify their emissions.

In Figure 17 the signatures produced by the TMSR-LF1 reactor are also shown with continuous removal of xenon and krypton. While the signatures do vary between the two cases due to a restricted build-up of longer-lived isotopes such as ^{133}Xe and ^{131m}Xe, in both cases the resulting signatures fall on the civilian source side of the discrimination line.

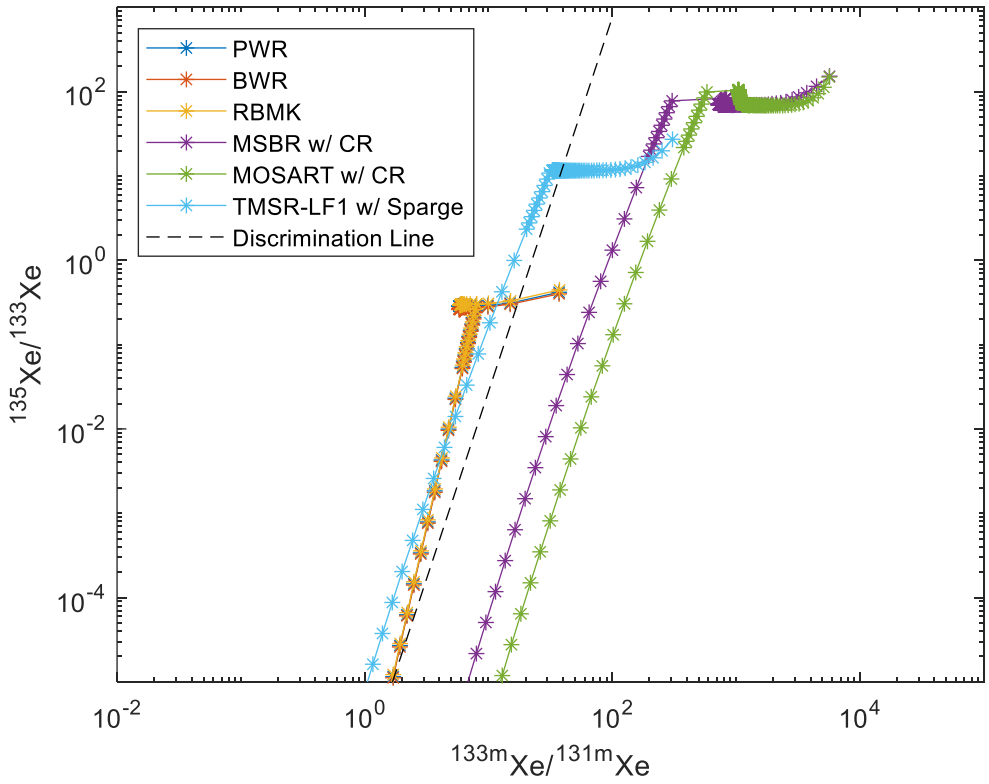

Figure 17. The four-isotope xenon ratio plots for various reactor designs for 300 days of operation. MSRs are shown with either continuous reprocessing and refueling (MSBR and MOSART) or sparging (TMSR-LF1). The DFR is not included in (b) due to a lack of specific reprocessing details. The traditional reactor signatures are shown for comparison.

5.2 Radioiodine comparison

In Figure 18 a multi-isotope ratio plot is shown for the three radioiodine isotopes ^{131}I, ^{133}I, and ^{135}I in the case that no reprocessing, refueling, or sparging occurs. Like in the xenon plots, a discrimination line has been proposed which may aid in the discrimination of civilian and weapon signatures (Kalinowski et al., 2014). In the case shown in Figure 18, the MSR signatures are nearly indistinguishable from each other and the conventional power reactors.

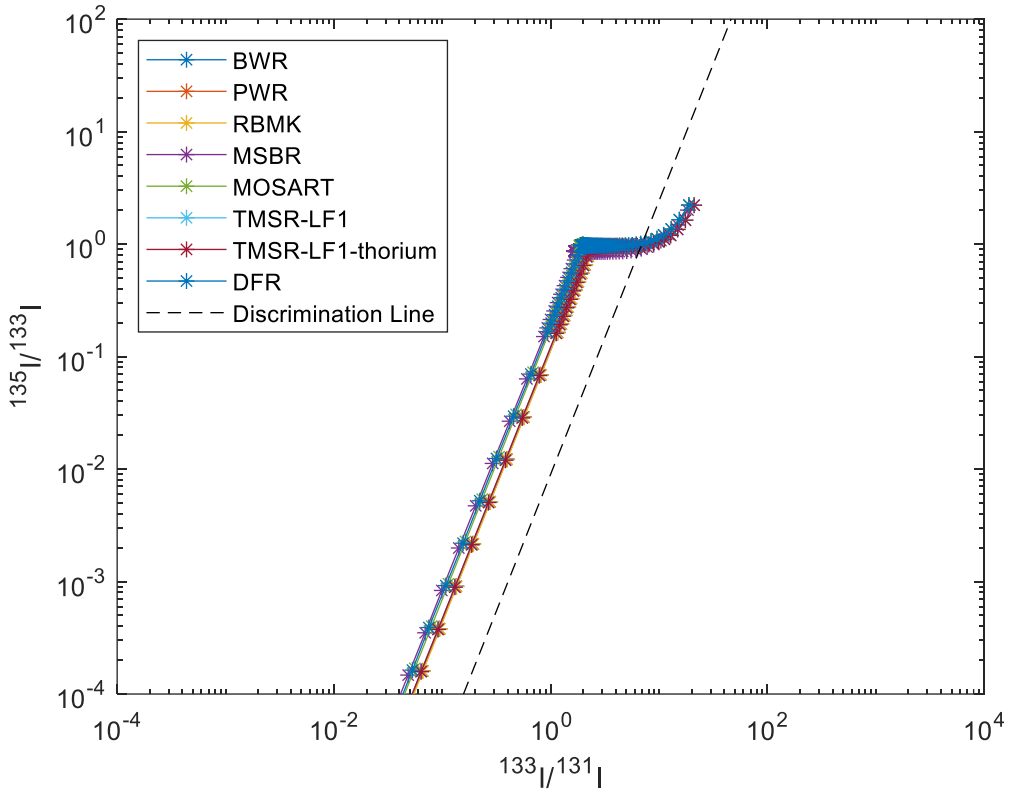

Figure 18. Radioiodine ratio plot for three light water reactors and molten salt reactors without continuous reprocessing or refueling.

However, like in the case of the xenon signatures, continuous reprocessing of the fuel salt shifts the MSR signatures below the discrimination line and into the region generally associated with nuclear weapons as shown in Figure 19. This is due to the continuous removal of parent isotopes, particularly isotopes of Te. During normal operations the emissions from both reactors lie almost directly over several measurements of radioiodine releases from nuclear explosive tests as shown in (Kalinowski et al., 2014). This highlights the potential difficulties MSRs may pose to the IMS.

The thorium-fueled MSBR sits significantly closer to the radioiodine discrimination line than the MOX-fueled MOSART due to the differing fission yields of the fissionable isotopes. This trend is not apparent in the case when no reprocessing occurs since the cumulative fission yields for the radioiodine isotopes do not vary dramatically between fissionable isotopes. However, the independent yields, which contribute more heavily in the case where parent isotopes are removed, vary by almost two orders of magnitude for the different fissionable isotopes used in the various MSR designs. The sparging case is not shown since in this scenario sparging only

removed noble gases and, since iodine does not have a noble gas parent, the noble gas sparging considered here has no effect on the iodine signatures of the TMSR-LF1 reactors.

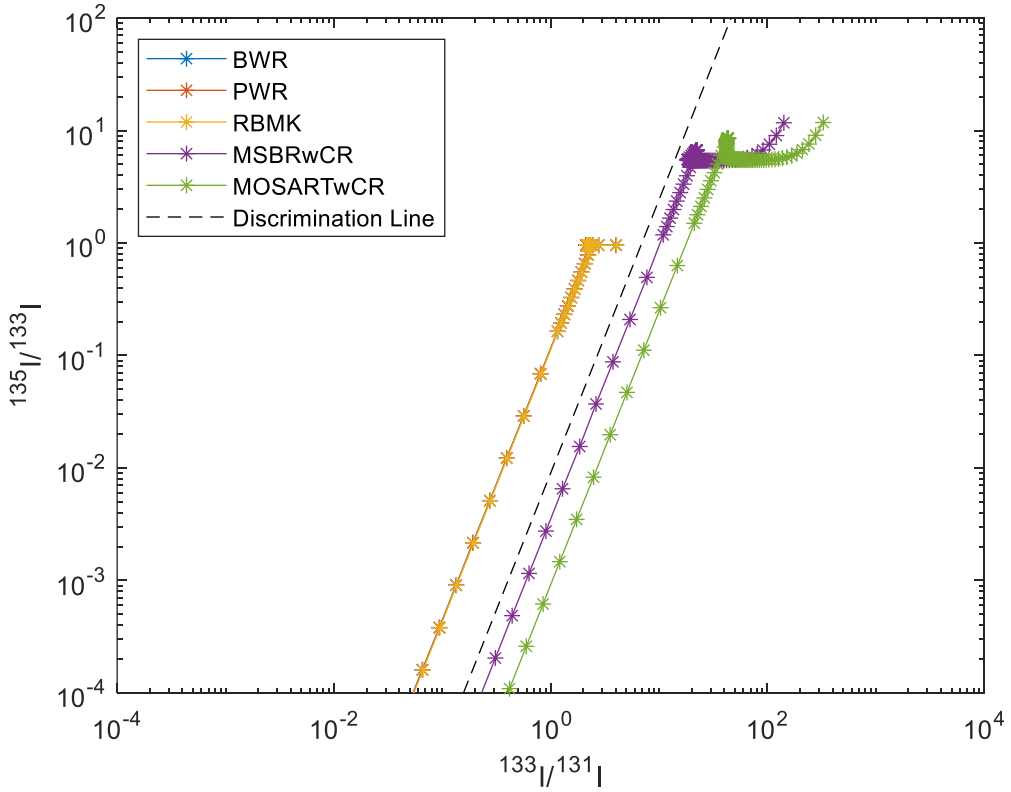

Figure 19. Radioiodine ratio plot for three light water reactors and two molten salt reactors with continuous reprocessing and refueling.

6.0 Implications for the IMS

When operated as closed units, the noble gas signatures of a molten salt reactors are not dissimilar to those of traditional power reactors. The impact on the IMS would be expected to be similar to that of currently operating nuclear power plants. Occasional releases of large quantities of radioxenon would be expected during maintenance and refueling cycles, but, these occurrences could be cross-correlated with reactor maintenance schedules and accounted for. In addition, in the case where the reactor is operated in a closed cycle with no reprocessing, refueling, or sparging of the fuel salt, the signature of the released radioxenons should be distinguishable from a nuclear weapon in the event that multiple isotopes are detected.

When operated as envisioned, with continuous reprocessing and refueling of the fuel salt, the potential impact of MSRs on the IMS increases dramatically. In cases where continuous removal of the xenon precursors (Sb, Te, I) occurs, the radioxenon signature of the MSRs shifts below the discrimination line and into the region typically associated with nuclear weapons.

More significant is the potential for large quantities of xenon being released daily from an MSR facility. In the event no xenon abatement is used, the large power reactors could release over 10^{16} Bq/d of ^{133}Xe while the smaller TMSR-LF1 could release 10^{15} Bq/d. For comparison, the highest average daily releases from the largest medical isotope emitters in 2005 was 1.60×10^{13} Bq/d (Saey, 2009). More recently, a voluntary xenon release threshold of 5×10^{9} Bq/d was proposed for medical isotope production facilities in order to minimize the impact of such facilities on the IMS (Bowyer et al., 2013). Using the same threshold, the minimum xenon hold-up time necessary after removal from the reactor was calculated. For the MSBR and MOSART, the minimum hold-up time necessary to restrict ^{133}Xe releases to the 5×10^{9} Bq/d was found to be 125 days, while the TMSR-LF1 required a hold-up of 95 days.

It is important to understand the IMS-relevant activation products that are produced during MSR operations. In the simulated example of TMSR-LF1, it was found that during reactor startup (< 28 hours), ^{24}Na (developed from irradiation of Na, Mg, and Al impurities) contributes the highest activity (saturating to ~2.4×10^{11} Bq). After 28 hours, ^{51}Cr (developed from irradiation of Fe and Cr corrosion products) has the highest activity (saturating to 4.8×10^{12} Bq). Interestingly, ^{42}K and ^{65}Zn had negligible activities (<10 Bq) for the initial 300-day operation period. However, the activity of these isotopes increased monotonically in time and reached 510 and 8.5 $\times10^{4}$ Bq, respectively, in 11,574 days since startup. The decay activity after reactor shutdown or fuel being removed from the reactor was initially (<136 days since shutdown) dominated by ^{51}Cr followed by ^{60}Co.

7.0 Recommendations for Future Work

Signatures/NEM focus:

The simulation results in this work only consider the primary fuel salt for four reactor types. Additional work is needed to understand the activation products in other areas including the secondary (coolant) loop and the cover gas. The cover gas may of particular interest since it is likely to be argon gas which, when activated in large volumes, may produce a measurable ^{37}Ar signature.

Additional work should also be undertaken to understand the impact of different abatement systems on the releases from MSRs. The work shown here only considered very simplistic abatement scenarios, while it is more likely that various technologies will be used which have varying impacts on the release of noble gases and particulates.

Activation Products:

The simulation results presented in this work give a complete overview of the activation products that develop due to irradiation of FLiBe fuel salt and are relevant to the IMS. It is therefore suggested that these results should be validated experimentally. Furthermore, since the cross-section of an isotope is a function of incident neutron's energy, the signature of these isotopes of interest should vary with the type/energy of irradiating neutron source. Future work shall investigate the impact of using various broad-energy (such as ^{252}Cf or fission neutrons from a nuclear reactor) and monoenergetic (such as neutrons from DD/DT fusion reactions) neutron sources on activation products' signatures. One key finding of this work was production of ^{42}K and ^{65}Zn; observed after a few years of operation of the nuclear reactor. The activity of these isotopes increased monotonically in time and reached 510 and 8.5×10^4 Bq, respectively, in 11574 days since startup. Though the activities contributed by these isotopes were negligible compared to other isotopes, it is envisaged that the signatures of these isotopes should vary with titanium and nickel concentrations. Irradiating several FLiBe samples with different titanium and nickel concentrations can justify this hypothesis.

8.0 Conclusion

Molten Salt Reactors have the potential to have a significant impact on the International Monitoring System. If they are treated like traditional power reactors and considered to be sealed systems for the duration of a cycle, then their xenon and iodine signatures emulate that of traditional power reactors and their emissions, while significant, would be infrequent. However, if the proposed on-line reprocessing, refueling, and sparging of the fuel salt are accounted for, their signatures shift dramatically and become nearly indistinguishable from a nuclear explosion. In addition, many of these proposed processing steps would result in frequent or continuous emissions of noble gases such as radioxenon in significant quantities up to 10^{15} Bq/d for a research reactor to 8×10^{16} Bq/d for a nuclear power plant. The monitoring community should take notice of these potential emissions and work to engage with designers and facilities to propose enhanced abatement of isotopes of interest, particularly radioxenon.

9.0 Acknowledgments

This research was funded by the National Nuclear Security Administration, Office of International Nuclear Safeguards (NNSA NA-241). The views expressed here do not necessarily reflect the opinion of the United States government, the United States Department of Energy, or the Pacific Northwest National Laboratory. Pacific Northwest National Laboratory is operated for the U.S. Department of Energy by Battelle under Contract DE-AC05-76RL01830.

10.0 References

Bowyer, S.M., Miley, H.S., Thompson, R.C., Hubbard, C.W., 1997. Automated particulate sampler for Comprehensive Test Ban Treaty verification (the DOE radionuclide aerosol sampler/analyzer). IEEE Trans. Nucl. Sci. 44, 551–556. https://doi.org/10.1109/23.603709

Bowyer, T.W., 2020. A Review of Global Radioxenon Background Research and Issues. Pure Appl. Geophys. https://doi.org/10.1007/s00024-020-02440-0

Bowyer, T.W., Biegalski, S.R., Cooper, M., Eslinger, P.W., Haas, D., Hayes, J.C., Miley, H.S., Strom, D.J., Woods, V., 2011. Elevated radioxenon detected remotely following the Fukushima nuclear accident. J. Environ. Radioact. 102, 681–687. https://doi.org/10.1016/j.jenvrad.2011.04.009

Bowyer, T.W., Kephart, R., Eslinger, P.W., Friese, J.I., Miley, H.S., Saey, P.R.J., 2013. Maximum reasonable radioxenon releases from medical isotope production facilities and their effect on monitoring nuclear explosions. J. Environ. Radioact. 115, 192–200. https://doi.org/10.1016/j.jenvrad.2012.07.018

Bowyer, T.W., Schlosser, C., Abel, K.H., Auer, M., Hayes, J.C., Heimbigner, T.R., McIntyre, J.I., Panisko, M.E., Reeder, P.L., Satorius, H., Schulze, J., Weiss, W., 2002. Detection and analysis of xenon isotopes for the comprehensive nuclear-test-ban treaty international monitoring system. J. Environ. Radioact. 59, 139–151. https://doi.org/10.1016/S0265-931X(01)00042-X

Burnett, J.L., 2019. Increasing the detection sensitivity of the Radionuclide Aerosol Sampler/Analyzer using a cosmic veto system. Nucl. Instruments Methods Phys. Res. Sect. A Accel. Spectrometers, Detect. Assoc. Equip. 944, 162473. https://doi.org/10.1016/j.nima.2019.162473

Burnett, J.L., Eslinger, P.W., Milbrath, B.D., 2019. The detectability of the Wigwam underwater nuclear explosion by the radionuclide stations of the International Monitoring System. J. Environ. Radioact. 208–209, 106030. https://doi.org/10.1016/j.jenvrad.2019.106030

Chen, C.Q., Xia, X. Bin, Zhang, Z.H., Cai, J., Li, C.Y., 2019. Radiological environmental impact analysis of a 2-MW thorium molten salt reactor during an accident. Nucl. Sci. Tech. 30. https://doi.org/10.1007/s41365-019-0605-3

Compere, E.L., Kirslis, S.S., Bohlmann, E.G., Blankenship, F.F., Grimes, W.R., 1975. Fission product behavior in the Molten Salt Reactor Experiment. Oak Ridge, TN (United States). https://doi.org/10.2172/4077644

Dolan, T.J., 2017. Molten Salt Reactors and Thorium Energy, Molten Salt Reactors and Thorium Energy. Woodhead Publishing.

Fontaine, J.P., Pointurier, F., Blanchard, X., Taffary, T., 2004. Atmospheric xenon radioactive isotope monitoring. J. Environ. Radioact. 72, 129–135. https://doi.org/10.1016/S0265-931X(03)00194-2

Guymon, R.H., Haubenreich, P.N., 1969. MSRE design and operations report. Part VI. Operating safety limits for the Molten-Salt Reactor Experiment (No. ORNL-TM-733). Oak Ridge, TN (United States). https://doi.org/10.2172/4580675

Haubenreich, P.N., Engel, J.R., 1970. Experience with the Molten-Salt Reactor Experiment. Nucl. Appl. Technol. 8, 118–136. https://doi.org/10.13182/NT8-2-118

Heuer, D., Merle-Lucotte, E., Allibert, M., Brovchenko, M., Ghetta, V., Rubiolo, P., 2014. Towards the thorium fuel cycle with molten salt fast reactors. Ann. Nucl. Energy 64, 421–429. https://doi.org/10.1016/j.anucene.2013.08.002

Holcomb, D., 2017. U.S. MSR Development Programs & Supportive Efforts. Gen IV Forum, PSI, Switzerland.

Huke, A., Ruprecht, G., Weißbach, D., Gottlieb, S., Hussein, A., Czerski, K., 2015. The Dual Fluid Reactor - A novel concept for a fast nuclear reactor of high efficiency. Ann. Nucl. Energy 80, 225–235. https://doi.org/10.1016/j.anucene.2015.02.016

IAEA, 2016. Advances in Small Modular Reactor Technology Developments - Status Report LFTR.

Ignatiev, V., Feynberg, O., Gnidoi, I., Konakov, S., Kormilitsyn, M., Merzliakov, A., Surenkov, A., Uglov, V., Zagnitko, A., 2015. MARS: Story on Molten Salt Actinide Recycler and Transmuter Development by Rosatom in Co-operation with Euratom.

Ignatiev, V., Feynberg, O., Gnidoi, I., Merzlyakov, A., Smirnov, V., Surenkov, A., Tretiakov, I., Zakirov, R., Afonichkin, V., Bovet, A., 2007. Progress in Development of Li, Be, Na/F Molten Salt Actinide Recycler & Transmuter Concept, in: Proceedings of ICAPP 2007.

International Atomic Energy Agency, 2019. Nuclear Power Reactors in the World. Ref. Data Ser. 2.

Kalinowski, M.B., Axelsson, A., Bean, M., Blanchard, X., Bowyer, T.W., Brachet, G., Hebel, S., McIntyre, J.I., Peters, J., Pistner, C., Raith, M., Ringbom, A., Saey, P.R.J., Schlosser, C., Stocki, T.J., Taffary, T., Kurt Ungar, R., 2010. Discrimination of Nuclear Explosions against Civilian Sources Based on Atmospheric Xenon Isotopic Activity Ratios. Pure Appl. Geophys. 167, 517–539. https://doi.org/10.1007/s00024-009-0032-1

Kalinowski, M.B., Liao, Y.Y., Pistner, C., 2014. Discrimination of Nuclear Explosions against Civilian Sources Based on Atmospheric Radioiodine Isotopic Activity Ratios. Pure Appl. Geophys. 171, 669–676. https://doi.org/10.1007/s00024-012-0564-7

Klix, A., Nishimura, H., Suzuki, A., Tanaka, T., Sato, S., Terai, T., Zaixin, L., Nishitani, T., Sagara, A., Muroga, T., 2005. Activation of flibe with 14 MeV DT neutrons. Proc. - Symp. Fusion Eng. 00, 20–23. https://doi.org/10.1109/FUSION.2005.252990

Li, J., Song, Y., Yin, J., Wang, D., 2017. Investigation on the effect of geometrical parameters on the performance of a venturi type bubble generator. Nucl. Eng. Des. 325, 90–96. https://doi.org/10.1016/j.nucengdes.2017.10.006

Liu, Y., Yan, R., Zou, Y., Yu, S., Zhou, B., Kang, X., Hu, J., Cai, X., 2020. Sensitivity/uncertainty

comparison and similarity analysis between TMSR-LF1 and MSR models. Prog. Nucl. Energy 122, 103289. https://doi.org/10.1016/j.pnucene.2020.103289

Lumbanraja, S.M., Liun, E., 2018. Implementation review of ThorCon molten salt reactor in Indonesia. J. Pengemb. Energi Nukl. 50.

Medici, F., 2001. The IMS radionuclide network of the CTBT. Radiat. Phys. Chem. 61, 689–690. https://doi.org/10.1016/S0969-806X(01)00375-9

Miley, H.S., Bowyer, S.M., Hubbard, C.W., McKinnon, A.D., Perkins, R.W., Thompson, R.C., Warner, R.A., 1998. A description of the DOE Radionuclide Aerosol Sampler/Analyzer for the Comprehensive Test Ban Treaty. J. Radioanal. Nucl. Chem. 235, 83–87. https://doi.org/10.1007/BF02385942

Miley, H.S., Burnett, J.L., Foxe, M.P., Haas, D.A., Keillor, M.E., Lowrey, J.D., Mayer, M.F., McIntyre, J.I., Wood, J.S., 2017. The potential detection of low-level aerosol isotopes from new civilian nuclear processes. Appl. Radiat. Isot. 126, 232–236. https://doi.org/https://doi.org/10.1016/j.apradiso.2017.02.033

National Institute of Standards and Technology, 2020. Neutron activation and scattering calculator [WWW Document].

National Nuclear Data Center, 2016. NuDat 2.7 [WWW Document].

Pater, M., 2019. Multiphysics simulations of Molten Salt Reactors using the Moltres Code. Université Paris-Saclay.

Rearden, B.T., Jessee, M.A., 2018. SCALE Code System. ORNL/TM-2005/39.

Ringbom, A., Larson, T., Axelsson, A., Elmgren, K., Johansson, C., 2003. SAUNA - A system for automatic sampling, processing, and analysis of radioactive xenon. Nucl. Instruments Methods Phys. Res. Sect. A Accel. Spectrometers, Detect. Assoc. Equip. 508, 542–553. https://doi.org/10.1016/S0168-9002(03)01657-7

Robertson, R.C., 1971. Conceptual Design Study of a Single-Fluid Molten-Salt Breeder Reactor (No. ORNL-4511). https://doi.org/10.2172/4030941

Robertson, R.C., 1965. MSRE DESIGN AND OPERATIONS REPORT. PART I. DESCRIPTION OF REACTOR DESIGN. Oak Ridge, TN. https://doi.org/10.2172/4654707

Rosenthal, M., 2010. An Account of Oak Ridge National Laboratory's Thirteen Nuclear Reactors, Ornl.

Rosenthal, M.W., Haubenreich, P.N., Briggs, R.B., 1972. The Development Status of Molten-Salt Breeder Reactors. Oak Ridge, TN.

Rykhlevskii, A., Bae, J.W., Huff, K.D., 2019. Modeling and simulation of online reprocessing in the thorium-fueled molten salt breeder reactor. Ann. Nucl. Energy 128, 366–379. https://doi.org/10.1016/j.anucene.2019.01.030

Saey, P.R.J., 2009. The influence of radiopharmaceutical isotope production on the global

radioxenon background. J. Environ. Radioact. 100, 396–406. https://doi.org/10.1016/j.jenvrad.2009.01.004

Schulze, J., Auer, M., Werzi, R., 2000. Low level radioactivity measurement in support of the CTBTO. Appl. Radiat. Isot. 53, 23–30. https://doi.org/10.1016/S0969-8043(00)00182-2

Sgro, P., 2018. TerraPower. Powering future reactor concepts. Atw Int. Zeitschrift fuer Kernenergie 63, 509–510.

Sheu, R.J., Chang, C.H., Chao, C.C., Liu, Y.W.H., 2013. Depletion analysis on long-term operation of the conceptual Molten Salt Actinide Recycler & Transmuter (MOSART) by using a special sequence based on SCALE6/TRITON. Ann. Nucl. Energy 53, 1–8. https://doi.org/10.1016/j.anucene.2012.10.017

UN, 1996. The Comprehensive Nuclear-Test-Ban Treaty.

VIJAYAN, P.K., BASAK, A., DULERA, I. V, VAZE, K.K., BASU, S., SINHA, R.K., 2015. Conceptual design of Indian molten salt breeder reactor. Pramana 85, 539–554. https://doi.org/10.1007/s12043-015-1070-0

Wang, X., Macian-Juan, R., 2018. Steady-state reactor physics of the dual fluid reactor concept. Int. J. Energy Res. 42, 4313–4334. https://doi.org/10.1002/er.4171

Wang, X., Zhang, Q., He, X., Du, Z., Seidl, M., Macian-Juan, R., Czerski, K., Dabrowski, M., 2019. Neutron physical feasibility of small modular design of dual fluid reactor. Int. Conf. Nucl. Eng. Proceedings, ICONE 2019-May.

Yin, J., Li, J., Ma, Y., Li, H., Liu, W., Wang, D., 2015. Study on the air core formation of a gas-liquid separator. J. Fluids Eng. Trans. ASME 137. https://doi.org/10.1115/1.4030198

Ying, D., Yang, H., Lyu, H., Tan, Y., Jing, F., Li, L., Xiao, F., Liu, J., Zhang, H., Yang, J., He, T., 2019. Activation of FLiBe coolant in the molten salt reactor. Ann. Nucl. Energy 129, 62–66. https://doi.org/10.1016/j.anucene.2019.01.038

Zhou, B., Yu, X.H., Liu, Y.F., Zou, Y., Yang, P., Yu, S.H., Kang, X.Z., Zhu, G.F., Yan, R., 2020a. Study on dynamic characteristics of activated products source term in secondary loop of integrated molten salt reactor. Radiat. Phys. Chem. 171. https://doi.org/10.1016/j.radphyschem.2020.108700

Zhou, B., Yu, X.H., Zou, Y., Yang, P., Yu, S.H., Liu, Y.F., Kang, X.Z., Zhu, G.F., Yan, R., 2020b. Study on dynamic characteristics of fission products in 2 MW molten salt reactor. Nucl. Sci. Tech. 31. https://doi.org/10.1007/s41365-020-0730-z

Appendix A – Reactor inventories of IMS relevant isotopes

Table A1. The calculated reactor inventory of CTBT relevant radioisotopes at 180 and 300 days of reactor operations for four molten salt reactor designs and an additional fuel loadout assuming no reprocessing, refueling, or sparging.

	Activity [Bq]									
	180 Days of Operation					300 Days of Operation				
Isotope	MSBR	MOSART	DFR	TMSR-LF1	TMSR-LF1 thorium	MSBR	MOSART	DFR	TMSR-LF1	TMSR-LF1 thorium
^{106m}Ag	4.34E+03	3.37E+07	4.15E+07	1.42E+02	1.35E+02	4.23E+04	4.25E+07	6.45E+07	2.41E+02	2.28E+02
^{108m}Ag	6.34E+04	1.19E+07	2.49E+08	2.21E+03	2.12E+03	1.69E+05	2.12E+07	6.37E+08	6.77E+03	6.47E+03
^{110m}Ag	1.58E+15	3.20E+15	1.06E+16	2.70E+09	2.59E+09	2.87E+15	6.53E+15	2.68E+16	7.58E+09	7.26E+09
^{111}Ag	2.12E+17	2.42E+17	2.17E+18	3.07E+13	2.96E+13	2.34E+17	2.53E+17	2.26E+18	3.41E+13	3.28E+13
^{74}As	2.88E+10	2.77E+09	2.39E+10	2.08E+05	2.03E+05	2.96E+10	2.33E+09	2.45E+10	3.43E+05	3.38E+05
^{76}As	3.74E+15	4.46E+13	1.64E+14	8.16E+08	7.91E+08	6.54E+15	6.63E+13	2.63E+14	1.20E+09	1.17E+09
^{196}Au	0	0	0	0	0	0	0	0	0	0
^{198}Au	0	0	0	0	0	0	0	0	0	0
^{133}Ba	1.06E+08	3.06E+07	1.81E+08	8.08E+02	4.38E+02	2.10E+08	5.57E+07	5.11E+08	3.87E+03	1.15E+03
^{140}Ba	6.10E+19	3.24E+18	2.99E+19	8.65E+15	7.58E+15	6.58E+19	3.01E+18	3.07E+19	8.64E+15	7.59E+15
^{115}Cd	1.39E+17	2.51E+16	2.27E+17	1.83E+13	1.78E+13	1.48E+17	2.52E+16	2.36E+17	1.87E+13	1.82E+13
^{115m}Cd	6.70E+15	1.42E+15	1.24E+16	9.78E+11	9.50E+11	8.03E+15	1.52E+15	1.42E+16	1.05E+12	1.02E+12
^{141}Ce	5.54E+19	3.03E+18	2.68E+19	7.95E+15	7.53E+15	6.31E+19	2.85E+18	2.84E+19	8.11E+15	7.69E+15
^{143}Ce	5.88E+19	2.62E+18	2.46E+19	8.27E+15	7.87E+15	6.24E+19	2.43E+18	2.51E+19	8.26E+15	7.86E+15
^{144}Ce	1.38E+19	8.46E+17	7.03E+18	2.71E+15	2.58E+15	2.27E+19	1.19E+18	1.08E+19	3.96E+15	3.76E+15
^{57}Co	0	0	0	0	0	0	0	0	0	0
^{58}Co	0	0	0	0	0	0	0	0	0	0
^{60}Co	0	0	0	0	0	0	0	0	0	0
^{51}Cr	0	0	0	0	0	0	0	0	0	0
^{132}Cs	1.22E+12	1.62E+11	6.57E+12	2.56E+09	1.08E+08	1.43E+12	1.57E+11	1.09E+13	4.37E+09	1.11E+08
^{134}Cs	9.24E+17	4.94E+16	1.34E+17	1.01E+12	2.73E+09	2.30E+18	1.27E+17	3.83E+17	2.80E+12	5.58E+09
^{136}Cs	1.03E+18	2.54E+17	8.82E+17	9.81E+12	6.87E+12	1.45E+18	3.93E+17	1.38E+18	1.27E+13	7.81E+12
^{137}Cs	6.12E+17	4.63E+16	3.77E+17	9.75E+13	2.65E+13	1.12E+18	7.40E+16	6.51E+17	1.62E+14	4.42E+13
^{152}Eu	3.56E+11	2.71E+12	2.11E+13	1.16E+09	1.10E+09	5.61E+11	8.44E+12	7.68E+13	4.99E+09	4.74E+09
^{152m}Eu	1.30E+14	1.73E+14	1.33E+15	7.29E+10	6.93E+10	2.03E+14	3.43E+14	2.94E+15	1.89E+11	1.79E+11

	Activity [Bq]									
	180 Days of Operation					300 Days of Operation				
Isotope	MSBR	MOSART	DFR	TMSR-LF1	TMSR-LF1-thorium	MSBR	MOSART	DFR	TMSR-LF1	TMSR-LF1 thorium
^{155}Eu	4.80E+15	7.15E+15	3.87E+16	2.87E+12	2.72E+12	1.05E+16	1.26E+16	5.26E+16	4.39E+12	4.16E+12
^{156}Eu	2.54E+18	1.36E+17	1.45E+18	3.28E+13	3.11E+13	5.85E+18	1.80E+17	1.78E+18	4.02E+13	3.82E+13
^{157}Eu	1.18E+18	6.31E+16	5.54E+17	1.03E+13	9.83E+12	2.65E+18	6.45E+16	5.71E+17	1.12E+13	1.06E+13
^{59}Fe	0	0	0	0	0	0	0	0	0	0
^{72}Ga	3.83E+15	6.00E+13	5.53E+14	4.38E+10	4.46E+10	3.86E+15	5.30E+13	5.63E+14	4.49E+10	4.63E+10
^{130}I	1.86E+18	1.89E+16	1.05E+17	8.66E+11	8.33E+11	3.22E+18	2.88E+16	1.72E+17	1.27E+12	1.22E+12
^{131}I	3.43E+19	2.13E+18	1.96E+19	4.05E+15	3.85E+15	3.63E+19	1.93E+18	2.01E+19	4.06E+15	3.87E+15
^{133}I	5.89E+19	4.02E+18	3.78E+19	9.35E+15	8.89E+15	6.26E+19	3.69E+18	3.85E+19	9.36E+15	8.90E+15
^{135}I	5.09E+19	3.89E+18	3.67E+19	8.79E+15	8.36E+15	5.45E+19	3.60E+18	3.74E+19	8.80E+15	8.37E+15
^{190}Ir	0	0	0	0	0	0	0	0	0	0
^{192}Ir	0	0	0	0	0	0	0	0	0	0
^{42}K	0	0	7.24E+04	0	0	0	0	5.55E+05	0	0
^{140}La	6.36E+19	3.28E+18	3.00E+19	8.66E+15	7.59E+15	7.07E+19	3.07E+18	3.09E+19	8.65E+15	7.60E+15
^{54}Mn	0	0	0	0	0	0	0	0	0	0
^{99}Mo	4.94E+19	3.61E+18	3.37E+19	8.52E+15	8.09E+15	5.32E+19	3.34E+18	3.45E+19	8.52E+15	8.10E+15
^{24}Na	1.77E+05	5.71E+18	0	0	0	1.37E+06	5.71E+18	0	0	0
^{95}Nb	3.52E+19	1.95E+18	1.64E+19	6.59E+15	6.26E+15	5.26E+19	2.29E+18	2.20E+19	8.39E+15	7.97E+15
^{147}Nd	1.43E+19	1.21E+18	1.14E+19	3.13E+15	2.98E+15	1.58E+19	1.13E+18	1.18E+19	3.13E+15	2.98E+15
^{239}Np	1.41E+16	3.86E+15	6.04E+20	4.57E+16	4.34E+16	8.17E+16	3.37E+15	5.87E+20	4.57E+16	4.33E+16
^{203}Pb	0	0	0	0	0	0	0	0	0	0
^{112}Pd	1.32E+17	1.00E+17	8.96E+17	2.20E+13	2.14E+13	1.41E+17	1.04E+17	9.18E+17	2.34E+13	2.27E+13
^{149}Pm	7.04E+18	8.60E+17	7.07E+18	1.50E+15	1.42E+15	8.43E+18	8.72E+17	7.44E+18	1.50E+15	1.43E+15
^{151}Pm	3.23E+18	4.79E+17	4.44E+18	5.93E+14	5.64E+14	3.54E+18	4.59E+17	4.56E+18	5.97E+14	5.68E+14
^{224}Ra	1.48E+12	1.20E+07	1.63E+06	1.76E+04	2.61E+08	3.08E+12	4.59E+07	7.33E+06	8.27E+04	1.22E+09

	Activity [Bq]									
	180 Days of Operation					300 Days of Operation				
Isotope	MSBR	MOSART	DFR	TMSR-LF1	TMSR-LF1 thorium	MSBR	MOSART	DFR	TMSR-LF1	TMSR-LF1 thorium
^{84}Rb	5.33E+11	4.79E+10	3.80E+11	3.88E+07	3.86E+06	5.83E+11	5.31E+10	4.54E+11	7.07E+07	4.83E+06
^{86}Rb	8.13E+16	1.85E+15	1.46E+16	6.49E+10	1.34E+10	1.53E+17	3.06E+15	2.64E+16	1.09E+11	1.72E+10
^{102}Rh	1.06E+09	8.34E+08	3.22E+11	6.91E+07	6.56E+07	1.93E+09	1.46E+09	9.85E+11	2.12E+08	2.02E+08
^{105}Rh	3.19E+18	3.29E+18	3.05E+19	1.42E+15	1.35E+15	3.58E+18	3.07E+18	3.12E+19	1.48E+15	1.40E+15
^{103}Ru	1.37E+19	3.93E+18	3.50E+19	4.14E+15	3.93E+15	1.70E+19	3.77E+18	3.80E+19	4.34E+15	4.12E+15
^{106}Ru	5.89E+17	8.47E+17	7.03E+18	1.77E+14	1.68E+14	1.02E+18	1.24E+18	1.11E+19	2.78E+14	2.64E+14
^{120m}Sb	2.74E+11	3.00E+10	1.63E+11	2.31E+06	2.28E+06	2.74E+11	3.18E+10	1.71E+11	3.82E+06	3.78E+06
^{122}Sb	2.36E+16	1.91E+15	5.68E+15	1.27E+10	1.23E+10	4.13E+16	2.94E+15	9.69E+15	2.12E+10	2.06E+10
^{124}Sb	1.96E+16	1.10E+15	2.87E+15	2.09E+10	3.17E+10	4.37E+16	2.14E+15	5.74E+15	2.99E+10	4.15E+10
^{125}Sb	1.02E+17	6.65E+15	5.31E+16	5.62E+12	5.36E+12	1.79E+17	1.01E+16	8.85E+16	9.20E+12	8.80E+12
^{126}Sb	1.15E+16	1.03E+15	7.81E+15	1.25E+12	1.19E+12	1.53E+16	1.10E+15	9.11E+15	1.26E+12	1.20E+12
^{127}Sb	5.03E+18	2.43E+17	2.22E+18	2.26E+14	2.16E+14	5.10E+18	2.13E+17	2.26E+18	2.31E+14	2.21E+14
^{128}Sb	9.81E+17	3.81E+16	3.43E+17	3.31E+13	3.16E+13	9.85E+17	3.25E+16	3.48E+17	3.39E+13	3.25E+13
^{46}Sc	0	0	0	0	0	0	0	0	0	0
^{47}Sc	0	0	0	0	0	0	0	0	0	0
^{153}Sm	8.38E+18	6.06E+17	3.32E+18	2.32E+14	2.21E+14	1.34E+19	7.84E+17	4.20E+18	2.39E+14	2.27E+14
^{156}Sm	1.28E+17	8.28E+16	7.77E+17	2.34E+13	2.22E+13	1.37E+17	7.94E+16	7.93E+17	2.47E+13	2.35E+13
^{125}Sn	5.03E+17	2.87E+16	2.61E+17	1.96E+13	1.87E+13	5.14E+17	2.53E+16	2.66E+17	2.02E+13	1.93E+13
^{91}Sr	6.33E+19	1.33E+18	1.26E+19	8.05E+15	7.27E+15	6.63E+19	1.20E+18	1.28E+19	8.01E+15	7.25E+15
^{99m}Tc	4.37E+19	3.20E+18	2.99E+19	7.55E+15	7.17E+15	4.71E+19	2.96E+18	3.05E+19	7.55E+15	7.18E+15
^{129m}Te	2.27E+18	1.14E+17	9.93E+17	1.26E+14	1.20E+14	2.51E+18	1.05E+17	1.05E+18	1.31E+14	1.25E+14
^{131m}Te	1.14E+19	4.69E+17	4.27E+18	5.88E+14	5.60E+14	1.15E+19	4.07E+17	4.34E+18	5.95E+14	5.69E+14
^{132}Te	4.62E+19	2.89E+18	2.70E+19	6.02E+15	5.72E+15	4.87E+19	2.64E+18	2.75E+19	6.03E+15	5.74E+15
^{168}Tm	1.62E+05	1.86E+07	1.77E+07	1.30E+02	1.24E+02	2.39E+05	4.26E+07	3.50E+07	3.07E+02	2.94E+02

	Activity [Bq]									
	180 Days of Operation					300 Days of Operation				
Isotope	MSBR	MOSART	DFR	TMSR-LF1	TMSR-LF1 thorium	MSBR	MOSART	DFR	TMSR-LF1	TMSR-LF1 thorium
^{237}U	1.27E+18	8.88E+14	3.72E+16	1.20E+14	1.14E+14	4.23E+18	1.46E+15	3.65E+16	1.35E+14	1.28E+14
^{187}W	0	0	0	0	0	0	0	0	0	0
^{131m}Xe	3.34E+17	2.23E+16	2.10E+17	4.39E+13	3.61E+09	3.67E+17	2.03E+16	2.16E+17	4.41E+13	3.63E+09
^{133}Xe	5.35E+19	3.82E+18	3.59E+19	8.85E+15	1.69E+12	5.75E+19	3.52E+18	3.66E+19	8.85E+15	1.69E+12
^{133m}Xe	1.86E+18	1.17E+17	1.10E+18	2.43E+14	1.20E+11	1.98E+18	1.07E+17	1.12E+18	2.43E+14	1.20E+11
^{135}Xe	1.58E+18	4.03E+18	3.83E+19	8.08E+15	1.94E+13	1.67E+18	3.71E+18	3.90E+19	8.10E+15	1.94E+13
^{88}Y	5.56E+11	5.50E+10	4.74E+11	1.09E+08	8.31E+07	7.35E+11	5.99E+10	6.96E+11	1.84E+08	1.21E+08
^{91}Y	4.92E+19	1.24E+18	1.06E+19	7.08E+15	6.39E+15	6.16E+19	1.25E+18	1.22E+19	7.78E+15	7.03E+15
^{93}Y	6.81E+19	2.06E+18	1.94E+19	8.79E+15	8.35E+15	7.14E+19	1.87E+18	1.97E+19	8.76E+15	8.33E+15
^{65}Zn	0	0	0	0	0	0	0	0	0	0
^{69m}Zn	3.71E+11	3.36E+10	3.03E+11	3.88E+06	3.79E+06	3.84E+11	3.00E+10	3.10E+11	4.72E+06	4.66E+06
^{89}Zr	2.40E+09	3.10E+08	3.30E+09	7.43E+11	6.78E+11	2.38E+09	2.75E+08	5.42E+09	7.43E+11	6.78E+11
^{95}Zr	4.70E+19	2.38E+18	2.03E+19	7.86E+15	7.46E+15	6.03E+19	2.45E+18	2.38E+19	8.79E+15	8.36E+15
^{97}Zr	5.44E+19	3.03E+18	2.84E+19	8.45E+15	8.02E+15	5.78E+19	2.79E+18	2.89E+19	8.44E+15	8.03E+15

Table A2. The calculated reactor inventory of CTBT relevant radioisotopes at 180 and 300 days of reactor operations for three molten salt reactor designs and an additional fuel loadout assuming continuous reprocessing and refueling of the MSBR and MOSART reactors and fuel sparging of the TMSR-LF1.

	Activity [Bq]							
	180 Days of Operation				300 Days of Operation			
Isotope	MSBR	MOSART	TMSR-LF1	TMSR-LF1 thorium	MSBR	MOSART	TMSR-LF1	TMSR-LF1 thorium
^{106m}Ag	4.74E-02	1.02E+03	1.42E+02	1.35E+02	2.71E-01	1.29E+03	2.41E+02	2.28E+02
^{108m}Ag	5.40E-03	3.33E+01	2.21E+03	2.12E+03	3.06E-02	4.16E+01	6.77E+03	6.47E+03
^{110m}Ag	1.85E+04	3.43E+06	2.70E+09	2.59E+09	1.74E+04	5.16E+06	7.58E+09	7.26E+09
^{111}Ag	4.82E+08	6.19E+09	3.07E+13	2.96E+13	4.08E+08	6.80E+09	3.41E+13	3.28E+13
^{74}As	3.95E+09	3.14E+04	2.08E+05	2.03E+05	2.62E+09	2.80E+04	3.43E+05	3.38E+05
^{76}As	1.38E+15	4.29E+08	8.16E+08	7.91E+08	1.61E+15	3.84E+08	1.20E+09	1.17E+09
^{196}Au	0	0	0	0	0	0	0	0
^{198}Au	0	0	0	0	0	0	0	0
^{133}Ba	4.05E+07	3.11E+07	4.53E+02	4.39E+02	5.30E+07	4.98E+07	1.18E+03	1.15E+03
^{140}Ba	7.04E+18	3.18E+18	8.57E+15	8.15E+15	5.28E+18	3.08E+18	8.56E+15	8.15E+15
^{115}Cd	6.01E+14	2.20E+10	1.83E+13	1.78E+13	4.89E+14	2.32E+10	1.87E+13	1.82E+13
^{115m}Cd	5.26E+13	6.54E+07	9.78E+11	9.50E+11	3.17E+13	6.96E+07	1.05E+12	1.02E+12
^{141}Ce	4.34E+18	3.30E+18	7.94E+15	7.56E+15	3.16E+18	3.24E+18	8.10E+15	7.71E+15
^{143}Ce	6.84E+18	3.38E+18	8.27E+15	7.87E+15	5.59E+18	3.31E+18	8.26E+15	7.86E+15
^{144}Ce	8.45E+17	8.14E+17	2.71E+15	2.58E+15	5.57E+17	1.03E+18	3.96E+15	3.76E+15
^{57}Co	0	0	0	0	0	0	0	0
^{58}Co	0	0	0	0	0	0	0	0
^{60}Co	0	0	0	0	0	0	0	0
^{51}Cr	0	0	0	0	0	0	0	0
^{132}Cs	1.25E+11	1.94E+11	1.18E+08	1.12E+08	9.78E+10	1.91E+11	1.24E+08	1.18E+08
^{134}Cs	7.33E+13	4.41E+13	4.69E+09	4.50E+09	6.07E+13	5.48E+13	1.08E+10	1.03E+10
^{136}Cs	1.11E+17	3.89E+16	7.16E+12	6.93E+12	7.80E+16	3.55E+16	8.05E+12	7.92E+12
^{137}Cs	3.49E+16	5.32E+15	7.77E+13	7.38E+13	4.21E+16	7.10E+15	1.29E+14	1.23E+14
^{152}Eu	2.91E+10	2.34E+12	1.16E+09	1.10E+09	2.08E+10	5.49E+12	4.99E+09	4.74E+09
^{152m}Eu	1.02E+13	1.61E+14	7.29E+10	6.93E+10	7.43E+12	2.61E+14	1.89E+11	1.79E+11
^{155}Eu	7.99E+14	6.88E+15	2.87E+12	2.72E+12	5.52E+14	1.06E+16	4.39E+12	4.16E+12
^{156}Eu	4.77E+17	1.57E+17	3.28E+13	3.11E+13	3.40E+17	1.96E+17	4.02E+13	3.82E+13
^{157}Eu	2.18E+17	8.35E+16	1.03E+13	9.83E+12	1.56E+17	8.90E+16	1.12E+13	1.06E+13
^{59}Fe	0	0	0	0	0	0	0	0
^{72}Ga	4.51E+14	3.60E+08	4.38E+10	4.46E+10	3.54E+14	3.24E+08	4.49E+10	4.63E+10
^{130}I	2.48E+15	2.17E+15	8.66E+11	8.33E+11	1.92E+15	1.88E+15	1.27E+12	1.22E+12
^{131}I	3.67E+16	1.40E+16	4.05E+15	3.85E+15	2.74E+16	1.25E+16	4.06E+15	3.87E+15
^{133}I	7.69E+17	5.93E+17	9.35E+15	8.89E+15	6.05E+17	5.24E+17	9.36E+15	8.90E+15
^{135}I	4.81E+18	3.82E+18	8.79E+15	8.36E+15	3.98E+18	3.69E+18	8.80E+15	8.37E+15
^{190}Ir	0	0	0	0	0	0	0	0
^{192}Ir	0	0	0	0	0	0	0	0
^{42}K	0	0	0	0	0	0	0	0

	Activity [Bq]							
	180 Days of Operation				300 Days of Operation			
Isotope	MSBR	MOSART	TMSR-LF1	TMSR-LF1 thorium	MSBR	MOSART	TMSR-LF1	TMSR-LF1 thorium
^{140}La	6.91E+18	3.18E+18	8.58E+15	8.16E+15	5.12E+18	3.09E+18	8.57E+15	8.16E+15
^{54}Mn	0	0	0	0	0	0	0	0
^{99}Mo	1.12E+14	8.53E+13	8.52E+15	8.09E+15	9.32E+13	8.33E+13	8.52E+15	8.10E+15
^{24}Na	1.77E+05	6.85E+18	0	0	1.37E+06	6.85E+18	0	0
^{95}Nb	3.51E+13	1.11E+13	6.59E+15	6.26E+15	2.24E+13	1.14E+13	8.39E+15	7.97E+15
^{147}Nd	1.47E+18	1.48E+18	3.13E+15	2.98E+15	1.19E+18	1.46E+18	3.13E+15	2.98E+15
^{239}Np	5.00E+15	5.64E+15	4.57E+16	4.34E+16	1.96E+16	5.14E+15	4.57E+16	4.33E+16
^{203}Pb	0	0	0	0	0	0	0	0
^{112}Pd	2.48E+12	1.96E+13	2.20E+13	2.14E+13	2.09E+12	2.19E+13	2.34E+13	2.27E+13
^{149}Pm	6.71E+17	1.09E+18	1.50E+15	1.42E+15	5.30E+17	1.13E+18	1.50E+15	1.43E+15
^{151}Pm	3.80E+17	6.20E+17	5.93E+14	5.64E+14	3.17E+17	6.22E+17	5.97E+14	5.68E+14
^{224}Ra	1.17E+11	1.40E+07	1.76E+04	2.61E+08	1.95E+11	5.27E+07	8.27E+04	1.22E+09
^{84}Rb	9.51E+10	5.57E+10	5.56E+06	5.41E+06	5.74E+10	6.44E+10	7.87E+06	7.76E+06
^{86}Rb	1.09E+15	1.14E+14	1.52E+10	1.58E+10	7.27E+14	1.09E+14	1.98E+10	2.14E+10
^{102}Rh	2.01E+02	2.09E+03	6.91E+07	6.56E+07	1.79E+02	2.34E+03	2.12E+08	2.02E+08
^{105}Rh	1.37E+09	1.52E+10	1.42E+15	1.35E+15	1.13E+09	1.44E+10	1.48E+15	1.40E+15
^{103}Ru	3.29E+11	8.01E+11	4.14E+15	3.93E+15	2.83E+11	7.71E+11	4.34E+15	4.12E+15
^{106}Ru	2.76E+10	4.09E+11	1.77E+14	1.68E+14	2.43E+10	4.03E+11	2.78E+14	2.64E+14
^{120m}Sb	8.87E+05	1.14E+06	2.31E+06	2.28E+06	6.89E+05	1.27E+06	3.82E+06	3.78E+06
^{122}Sb	1.39E+09	7.40E+08	1.27E+10	1.23E+10	1.07E+09	7.01E+08	2.12E+10	2.06E+10
^{124}Sb	6.23E+07	1.30E+08	2.09E+10	3.17E+10	5.24E+07	1.36E+08	2.99E+10	4.15E+10
^{125}Sb	1.96E+10	1.53E+08	5.62E+12	5.36E+12	1.50E+10	1.39E+08	9.20E+12	8.80E+12
^{126}Sb	1.01E+10	9.34E+09	1.25E+12	1.19E+12	8.33E+09	8.25E+09	1.26E+12	1.20E+12
^{127}Sb	2.41E+13	8.49E+11	2.26E+14	2.16E+14	1.90E+13	7.65E+11	2.31E+14	2.21E+14
^{128}Sb	3.39E+13	1.38E+13	3.31E+13	3.16E+13	2.63E+13	1.22E+13	3.39E+13	3.25E+13
^{46}Sc	0	0	0	0	0	0	0	0
^{47}Sc	0	0	0	0	0	0	0	0
^{153}Sm	5.68E+17	7.18E+17	2.32E+14	2.21E+14	4.01E+17	8.55E+17	2.39E+14	2.27E+14
^{156}Sm	1.53E+16	1.08E+17	2.34E+13	2.22E+13	1.30E+16	1.10E+17	2.47E+13	2.35E+13
^{125}Sn	5.78E+16	6.00E+11	1.96E+13	1.87E+13	4.28E+16	5.60E+11	2.02E+13	1.93E+13
^{91}Sr	6.56E+18	1.49E+18	8.01E+15	7.62E+15	5.33E+18	1.41E+18	7.97E+15	7.59E+15
^{99m}Tc	6.33E+10	4.90E+10	7.55E+15	7.17E+15	5.29E+10	4.78E+10	7.55E+15	7.18E+15
^{129m}Te	1.08E+11	2.36E+09	1.26E+14	1.20E+14	8.32E+10	2.53E+09	1.31E+14	1.25E+14
^{131m}Te	1.33E+14	5.52E+13	5.88E+14	5.60E+14	1.04E+14	4.97E+13	5.95E+14	5.69E+14
^{132}Te	1.97E+14	8.24E+13	6.02E+15	5.72E+15	1.57E+14	7.83E+13	6.03E+15	5.74E+15
^{168}Tm	1.11E+04	2.88E+07	1.30E+02	1.24E+02	1.50E+04	6.71E+07	3.07E+02	2.94E+02
^{237}U	3.71E+17	1.10E+15	1.20E+14	1.14E+14	8.26E+17	1.89E+15	1.35E+14	1.28E+14

	Activity [Bq]							
	180 Days of Operation				300 Days of Operation			
Isotope	MSBR	MOSART	TMSR-LF1	TMSR-LF1 thorium	MSBR	MOSART	TMSR-LF1	TMSR-LF1 thorium
^{187}W	0	0	0	0	0	0	0	0
^{131m}Xe	5.75E+09	2.28E+09	3.80E+10	3.61E+10	4.30E+09	2.03E+09	3.81E+10	3.62E+10
^{133}Xe	2.33E+13	1.78E+13	1.77E+13	1.68E+13	1.83E+13	1.57E+13	1.77E+13	1.69E+13
^{133m}Xe	4.61E+12	2.48E+12	1.25E+12	1.19E+12	3.58E+12	2.18E+12	1.26E+12	1.19E+12
^{135}Xe	1.85E+15	1.42E+15	2.16E+14	2.05E+14	1.52E+15	1.37E+15	2.16E+14	2.06E+14
^{88}Y	3.44E+10	5.39E+10	1.04E+08	9.60E+07	2.07E+10	5.53E+10	1.71E+08	1.59E+08
^{91}Y	3.02E+18	1.11E+18	7.05E+15	6.70E+15	2.05E+18	1.12E+18	7.74E+15	7.37E+15
^{93}Y	8.01E+18	2.66E+18	8.79E+15	8.36E+15	6.55E+18	2.54E+18	8.76E+15	8.34E+15
^{65}Zn	0	0	0	0	0	0	0	0
^{69m}Zn	4.50E+10	1.20E+07	3.88E+06	3.79E+06	3.77E+10	1.12E+07	4.72E+06	4.66E+06
^{89}Zr	2.66E+08	3.97E+08	7.43E+11	6.78E+11	2.02E+08	3.72E+08	7.43E+11	6.78E+11
^{95}Zr	7.73E+18	2.45E+18	7.86E+15	7.46E+15	4.93E+18	2.52E+18	8.79E+15	8.36E+15
^{97}Zr	6.55E+18	3.92E+18	8.45E+15	8.02E+15	5.42E+18	3.80E+18	8.44E+15	8.03E+15

Table A3. The calculated reactor inventory of CTBT relevant radioisotopes at 180 and 300 days of reactor operations for BWR, PWR, and RBMK reactors assuming a 100 MTU fuel load.

	Activity [Bq]					
	180 Days of Operation			300 Days of Operation		
Isotope	BWR	PWR	RBMK	BWR	PWR	RBMK
^{106m}Ag	1.51E+06	1.57E+06	6.01E+05	2.13E+06	2.32E+06	8.94E+05
^{108m}Ag	3.97E+07	4.16E+07	3.67E+06	1.39E+08	1.60E+08	1.34E+07
^{110m}Ag	2.61E+14	2.77E+14	4.83E+13	8.07E+14	9.26E+14	1.66E+14
^{111}Ag	8.75E+16	9.05E+16	3.45E+16	1.14E+17	1.23E+17	4.63E+16
^{74}As	1.79E+09	1.89E+09	5.13E+08	2.71E+09	3.09E+09	7.88E+08
^{76}As	1.58E+13	1.75E+13	4.14E+12	2.49E+13	3.03E+13	7.02E+12
^{196}Au	0	0	0	0	0	0
^{198}Au	0	0	0	0	0	0
^{133}Ba	7.01E+07	7.64E+07	3.44E+06	4.92E+08	6.14E+08	1.69E+07
^{140}Ba	7.55E+18	7.53E+18	3.82E+18	7.45E+18	7.40E+18	3.77E+18
^{115}Cd	2.78E+16	2.87E+16	1.12E+16	2.96E+16	3.19E+16	1.23E+16
^{115m}Cd	1.46E+15	1.49E+15	5.81E+14	1.68E+15	1.78E+15	6.84E+14
^{141}Ce	6.97E+18	6.95E+18	3.53E+18	7.02E+18	6.97E+18	3.56E+18
^{143}Ce	7.01E+18	6.97E+18	3.58E+18	6.86E+18	6.77E+18	3.50E+18
^{144}Ce	2.34E+18	2.34E+18	1.19E+18	3.35E+18	3.33E+18	1.71E+18
^{57}Co	0	0	0	0	0	0
^{58}Co	0	0	0	0	0	0
^{60}Co	0	0	0	0	0	0
^{51}Cr	0	0	0	0	0	0
^{132}Cs	1.13E+13	1.22E+13	1.22E+12	1.86E+13	2.28E+13	2.20E+12
^{134}Cs	2.78E+16	2.94E+16	6.34E+15	7.30E+16	8.19E+16	1.78E+16
^{136}Cs	3.57E+16	3.87E+16	1.27E+16	5.33E+16	6.18E+16	1.93E+16
^{137}Cs	8.78E+16	8.77E+16	4.41E+16	1.46E+17	1.46E+17	7.32E+16
^{152}Eu	2.18E+12	2.59E+12	1.16E+12	3.43E+12	4.42E+12	2.06E+12
^{152m}Eu	1.96E+14	2.09E+14	1.04E+14	2.63E+14	2.83E+14	1.48E+14
^{155}Eu	1.74E+15	1.73E+15	9.31E+14	2.91E+15	2.87E+15	1.37E+15
^{156}Eu	1.16E+17	1.17E+17	4.41E+16	1.76E+17	1.83E+17	6.29E+16
^{157}Eu	2.71E+16	2.82E+16	1.05E+16	3.44E+16	3.77E+16	1.35E+16
^{59}Fe	0	0	0	0	0	0
^{72}Ga	7.40E+13	7.71E+13	2.85E+13	7.93E+13	8.67E+13	3.20E+13
^{130}I	1.08E+16	1.03E+16	3.62E+15	1.89E+16	1.83E+16	6.40E+15
^{131}I	3.82E+18	3.82E+18	1.89E+18	3.87E+18	3.89E+18	1.92E+18
^{133}I	8.30E+18	8.29E+18	4.17E+18	8.29E+18	8.26E+18	4.16E+18
^{135}I	7.93E+18	7.92E+18	3.97E+18	7.93E+18	7.91E+18	3.97E+18
^{190}Ir	0	0	0	0	0	0
^{192}Ir	0	0	0	0	0	0
^{42}K	0	0	0	0	0	0

	Activity [Bq]					
	180 Days of Operation			300 Days of Operation		
Isotope	BWR	PWR	RBMK	BWR	PWR	RBMK
^{140}La	7.59E+18	7.57E+18	3.84E+18	7.52E+18	7.46E+18	3.80E+18
^{54}Mn	0	0	0	0	0	0
^{99}Mo	7.64E+18	7.62E+18	3.83E+18	7.62E+18	7.59E+18	3.82E+18
^{24}Na	0	0	0	0	0	0
^{95}Nb	5.63E+18	5.62E+18	2.87E+18	7.02E+18	6.97E+18	3.58E+18
^{147}Nd	2.73E+18	2.73E+18	1.38E+18	2.71E+18	2.69E+18	1.37E+18
^{239}Np	5.78E+19	6.49E+19	2.68E+19	5.58E+19	6.78E+19	2.77E+19
^{203}Pb	0	0	0	0	0	0
^{112}Pd	5.03E+16	5.22E+16	1.97E+16	6.03E+16	6.56E+16	2.44E+16
^{149}Pm	1.58E+18	1.58E+18	7.35E+17	1.68E+18	1.72E+18	7.73E+17
^{151}Pm	6.14E+17	6.18E+17	2.94E+17	6.40E+17	6.53E+17	3.07E+17
^{224}Ra	1.77E+07	1.75E+07	7.84E+06	1.04E+08	1.08E+08	4.13E+07
^{84}Rb	2.60E+11	2.81E+11	1.51E+10	4.64E+11	5.61E+11	2.78E+10
^{86}Rb	1.23E+15	1.35E+15	3.10E+14	2.02E+15	2.44E+15	5.53E+14
^{102}Rh	5.30E+11	5.52E+11	5.24E+10	1.57E+12	1.80E+12	1.70E+11
^{105}Rh	2.19E+18	2.26E+18	9.79E+17	2.54E+18	2.70E+18	1.15E+18
^{103}Ru	4.44E+18	4.46E+18	2.11E+18	4.94E+18	5.03E+18	2.34E+18
^{106}Ru	3.20E+17	3.23E+17	1.34E+17	5.85E+17	6.06E+17	2.46E+17
^{120m}Sb	1.90E+10	2.09E+10	2.47E+09	3.08E+10	3.83E+10	3.82E+09
^{122}Sb	5.59E+14	6.25E+14	1.22E+14	9.17E+14	1.15E+15	2.22E+14
^{124}Sb	2.53E+14	2.76E+14	6.09E+13	5.05E+14	6.08E+14	1.29E+14
^{125}Sb	6.85E+15	6.89E+15	2.99E+15	1.18E+16	1.20E+16	5.17E+15
^{126}Sb	1.28E+15	1.29E+15	6.19E+14	1.36E+15	1.39E+15	6.52E+14
^{127}Sb	2.70E+17	2.74E+17	1.26E+17	2.95E+17	3.04E+17	1.38E+17
^{128}Sb	4.07E+16	4.13E+16	1.90E+16	4.50E+16	4.65E+16	2.12E+16
^{46}Sc	0	0	0	0	0	0
^{47}Sc	0	0	0	0	0	0
^{153}Sm	5.05E+17	5.24E+17	1.77E+17	6.87E+17	7.59E+17	2.37E+17
^{156}Sm	4.54E+16	4.67E+16	1.92E+16	5.46E+16	5.83E+16	2.35E+16
^{125}Sn	2.62E+16	2.66E+16	1.19E+16	2.95E+16	3.07E+16	1.35E+16
^{91}Sr	6.45E+18	6.39E+18	3.34E+18	6.15E+18	6.00E+18	3.20E+18
^{99m}Tc	6.72E+18	6.71E+18	3.37E+18	6.70E+18	6.68E+18	3.36E+18
^{129m}Te	1.37E+17	1.38E+17	6.50E+16	1.50E+17	1.54E+17	7.13E+16
^{131m}Te	6.25E+17	6.28E+17	3.04E+17	6.65E+17	6.76E+17	3.25E+17
^{132}Te	5.58E+18	5.58E+18	2.77E+18	5.62E+18	5.62E+18	2.79E+18
^{168}Tm	4.38E+06	4.73E+06	1.40E+05	8.98E+06	1.12E+07	3.04E+05
^{237}U	1.14E+18	1.29E+18	2.40E+17	1.38E+18	1.75E+18	3.28E+17

	Activity [Bq]					
	180 Days of Operation			300 Days of Operation		
Isotope	BWR	PWR	RBMK	BWR	PWR	RBMK
^{187}W	0	0	0	0	0	0
^{131m}Xe	4.16E+16	4.17E+16	2.05E+16	4.29E+16	4.32E+16	2.10E+16
^{133}Xe	8.39E+18	8.38E+18	4.21E+18	8.38E+18	8.36E+18	4.21E+18
^{133m}Xe	2.47E+17	2.47E+17	1.23E+17	2.49E+17	2.50E+17	1.24E+17
^{135}Xe	2.27E+18	2.42E+18	1.26E+18	2.19E+18	2.39E+18	1.23E+18
^{88}Y	2.22E+11	2.38E+11	1.58E+10	6.23E+11	7.35E+11	4.11E+10
^{91}Y	5.98E+18	5.95E+18	3.08E+18	6.27E+18	6.18E+18	3.26E+18
^{93}Y	7.25E+18	7.20E+18	3.72E+18	7.00E+18	6.88E+18	3.61E+18
^{65}Zn	0	0	0	0	0	0
^{69m}Zn	2.28E+10	2.42E+10	7.70E+09	2.77E+10	3.12E+10	1.03E+10
^{89}Zr	2.48E+09	2.78E+09	2.23E+08	6.93E+09	8.87E+09	6.13E+08
^{95}Zr	6.67E+18	6.65E+18	3.40E+18	7.30E+18	7.24E+18	3.73E+18
^{97}Zr	7.29E+18	7.27E+18	3.69E+18	7.21E+18	7.16E+18	3.64E+18

Pacific Northwest National Laboratory

902 Battelle Boulevard
P.O. Box 999
Richland, WA 99354
1-888-375-PNNL (7665)

www.pnnl.gov